Supporting Information

How to Evaluate Aromaticity under Pressure? Benzene as a Benchmark System

Jochen Eckhoudt,[a‡] Alexander Dellwisch,[b‡] Annelene Plump,[b] Felix Zeller,[b] Tim Neudecker,[b,c,d*] Frank De Proft,[a] and Mercedes Alonso[a*]

[a] *Vrije Universiteit Brussel, Pleinlaan 2, Elsene, Belgium*

[b] *University of Bremen, Institute for Physical and Theoretical Chemistry, Leobener Straße 6, Bremen, Germany*

[c] *Bremen Center for Computational Materials Science, University of Bremen, Am Fallturm 1, D-28359 Bremen, Germany*

[d] *MAPEX Center for Materials and Processes, University of Bremen, Bibliothekstraße 1, D-28359 Bremen, Germany*

‡ *These authors contributed equally to this work*

Contents

1 Full Computational Details

As a first step in investigating the aromaticity behavior of benzene under pressure, geometry optimizations at the level of theory B3LYP[1,2]-D3[3]/cc-pVTZ[4] were carried out using two pressure models, the eXtended Hydrostatic Compression Force Field (X-HCFF)[5,6] and Gaussians On Surface Tesserae Simulate HYdrostatic Pressure (GOSTSHYP),[7,8] implemented in the Q-Chem 6.0 software.[9] The pressure range extended from 0 to 100 GPa, with optimizations carried out in 5 GPa increments. For both pressure methods, 110 tessellation points were used for both atom types, with the scaling factor in X-HCFF set to 1.0.

For GOSTSHYP, the cavity was adjusted to better describe electron density compression by adjusting the van der Waals radii of carbon and hydrogen to match the 0.001 e/bohr^3 isodensity surface of benzene.[10] A cube file of the optimized geometry was generated, and the isodensity surface was extracted as a point cloud using a Python 3.11 script.[11] As the starting cavity, the van der Waals surface of benzene, centered on atomic positions using known radii of carbon (1.70 Å) and hydrogen (1.20 Å), was used.[12] The RMSE of the shortest distances from the cavity to the 0.001 e/bohr^3 isodensity surface was then calculated, and a minimization was performed using a related steepest descent algorithm in Python. The optimized van der Waals radii were determined to be 2.0478 Å for carbon and 1.3919 Å for hydrogen (RMSE $<$ 0.054 Å). In some cases, the Bondi set of atomic radii is used instead, but they yield comparable results owing to the similar R_H/R_C ratio.

A comparison of the aromaticity between a gas phase molecule and a single molecule within the crystal was achieved by performing plane-wave-based DFT calculations under pressure on the crystal structure of benzene using the Vienna Ab initio Simulation Package (VASP) 3.6.0.[13,14] The starting structure was taken from the literature (.cif file[15]), and a POSCAR file was generated using VESTA. The projector augmented-wave (PAW) method was used to describe electron interactions in combination with the GGA-PBE exchange-correlation functional.[16] Corresponding PAW pseudopotentials[17,18] were employed for carbon (08-Apr-2002) and hydrogen (15-Jun-2001). The wavefunctions were represented using a plane-wave energy cutoff of 400 eV. The Brillouin zone was sampled using a Gamma-centered 3×3×2 k-point mesh. Electronic self-consistency was converged to an energy tolerance of 10^{-6} eV (EDIFF), using Gaussian smearing with ISMEAR=0 and

SIGMA=0.05 eV. Geometry optimizations were performed using the conjugate gradient algorithm (IBRION=2), with both atomic positions and cell parameters relaxed (ISIF=3). After optimization, the geometries of individual molecules were extracted at each pressure point.

Based on the bond lengths obtained from the crystal structure, the bond length alternation (BLA) index was calculated at each pressure point using two different definitions.[19–22]

To reliably apply the HOMA (Harmonic Oscillator Model of Aromaticity) index[23,24] to the benzene molecule in the crystal under pressure, reference values for a C–C single bond and a C=C double bond were initially determined. Two approaches were used, each based on different reference molecules. In the first approach, ethane and ethene were used as the simplest reference compounds. Pressure-dependent calculations (B3LYP-D3/cc-pVTZ) using GOSTSHYP were performed from 0 to 100 GPa in 5 GPa steps. The scaling factor was set to 1.3, and 110 tessellation points per atom type were used.

In the second approach, butadiene containing both bond types, was used as a reference structure, and corresponding pressure calculations were also performed via GOSTSHYP with the same settings. Following geometry optimization, both carbon–carbon bond lengths were evaluated and subsequently used to calculate the HOMA index of the crystal-phase molecule by applying the pressure-dependent parameters α and the reference bond length R_{ref}.

The aromatic stabilization energies were computed as reaction energies for a hypohomodesmotic and homodesmotic reaction (see main text). The energies were computed at the B3LYP-D3/cc-pVTZ level of theory and the Bondi set of van der Waals radii with a TSSF of 1.3 were used for all molecules. Symmetry was turned off, wavefunctions were converged to an error below 10^{-7} E_h and 110 points were used for the Lebedev grids underlying the X-HCFF and GOSTSHYP models.

For the determination of the ring critical point (RCP) properties[25–28] as electronic aromaticity indices, wavefunction files (.fchk files) were generated for the optimized benzene structures in both environments via single-point calculations (B3LYP-D3/cc-pVTZ) via Q-Chem. These were subsequently imported into the Multiwfn 3.8 software, and Quantum Theory of Atoms in Molecules (QTAIM) analyses were performed. For comparison, RCP properties were also calculated for cyclohexane using the same procedure after com-

pression with GOSTSHYP. Standard van der Waals radii for carbon and hydrogen from the Bondi set were applied, along with a scaling factor of 1.3.

Delocalization indices were computed from the formatted checkpoint files (after conversion to the .wfn file format by Multiwfn) with the AIMAll software (version 19.10.12).[29] This program computes the overlap integrals in the QTAIM basins and these form the input for the multicenter indices which were computed with the ESI-3D software.[30] Because the QTAIM partition combined with GOSTSHYP method resulted in non-nuclear attractors at a significant distance from the molecule but with negligible associated electron density for large pressures, the multicenter indices for 95 and 100 GPa could not be calculated for technical reasons. Additional spatial partitions (Hirshfeld[31] and Topological Fuzzy Voronoi Cells[32]) were also considered in the computation of the multicenter indices and the overlap integrals for these were calculated by the APOST-3D program.[33] For the latter partitions, only the variant with Bondi radii was considered.

From the formatted checkpoint files, the linear response function was computed with an in-house code at both the IPA and LDA level and the LRF matrix was condensed with the Hirshfeld partition.[34] Pressurized atomic densities were computed for GOSTSHYP at the same level of theory as the benzene molecule. For the designation of the *ortho*, *meta* and *para* carbons, each ring position was considered as the ipso carbon and the average was taken to minimize numerical artefacts. In retrospect, this additional step is likely unnecessary.

To determine nucleus-independent chemical shift values (NICS(0), $\mathrm{NICS(0)_{zz}}$, NICS(1), and $\mathrm{NICS(1)_{zz}}$)[35–37] for the pressure-optimized structures of the gas phase and crystal molecule, NMR calculations (B3LYP-D3/cc-pVTZ) were performed using Q-Chem. Ghost atoms were placed at the geometric center of the ring and 1 Å above it. The convergence thresholds for Level-1 and Level-2 iterations were each set to 10^{-4}, while the SCF threshold was set to 10^{-7} $\mathrm{E_h}$. Symmetry recognition and automatic reorientation of molecules were deactivated. NICS values were obtained from the shielding tensors.

Infinitely-thin conducting line of current models were fitted to $\mathrm{NICS(x)_{zz}}$ linescans from the ring center perpendicular to the plane up to 10 Å for 0, 20, 40, 60, 80 and 100 GPa.[38–40] The shielding tensors were obtained in the same manner as the NICS indices, but with the Bondi radii used in the pressure models. Four different fitting variants (LSQ, LSQ5A, WSQY2 and WSQVAR) and six different models (ICLOC1, ICLOC2Z,

ICLOC4, ICLOC4hex, TCLOC1 and ICLOC2XY) were applied to the NICS linescans and performed by a Python 3.9 script using SciPy 1.8.0. The ICLOC1 model consists of one loop in the plane of the molecule. The ICLOC2Z model places two loops carrying the same current symmetrically above and below the plane. The ICLOC2XY model places a larger loop to carry the diatropic current and a smaller loop for the paratropic current both in the plane of the molecule. The ICLOC4 model combines the last two in one model. The ICLOC4hex model replaces the circular loops in the ICLOC4 model by hexagonal loops. The TCLOC model replaces the infinitely thin loop in the basic ICLOC1 model with a toroidal loop where the current is spread out over space. The LSQ fitting variant performs a simple least squares fit of the data to the model. The LSQ5A fitting variant is limited to 5 Å instead of 10 Å and was attempted to improve the model fit in the region where the data showed the most variation. For the same reason, the WSQY2 variant performs a weighted least squares fit where the weights are equal to the value of the NICSzz squared and the WSQVAR performs a weighted least squares fit where the weights are equal to the variance of the $NICS_{zz}$ between the different pressures. The parameters were analyzed for those models which resulted in a stable fit and upon visual inspection showed a meaningful difference in fitting quality between the 0 and 20 GPa cases. The best performing TCLOC model was repeated with the least squares fit variant for NICS linescans with the isosurface fitted radii.

Analytical ring currents were computed using the GIMIC program. Perturbed density matrices were obtained from Q-Chem 6.0 or Gaussian16 calculations. The Bondi radii were used in the pressure models and a C++ GitHub script was used to convert the binary Q-Chem files to the GIMIC format.[41] Integrations of the ring currents were performed over the plane bisecting the C-C bonds between the ring center and up to 12 Bohr extending from the C-C bond. These were performed over every bond and averaged to reduce numerical artifacts. The integration could be split up in both vertical and horizontal sections of 0.1 Bohr to visualize the current profile across the bond parallel and perpendicular to the plane of the aromatic ring.

To exclude any influence of long-range interactions on the aromaticity descriptors under pressure, additional pressure calculations were performed on the gas phase molecule with GOSTSHYP using CAM-B3LYP[42] as the exchange-correlation functional and the optimized van der Waals radii for carbon and hydrogen. Consistent with the other calcu-

lations, Grimme's D3 dispersion correction and the cc-pVTZ basis set were employed. On this basis, the HOMA index, RCP properties, PDI and multicenter indices were evaluated, all displaying the same trends as obtained with the B3LYP functional. In addition, a technical limitation of the Q-Chem code prevents the calculation of the NICS indices using the CAM-B3LYP functional. Furthermore, the self-interaction error associated with the standard B3LYP functional is expected to be negligible for benzene, owing to its relatively small molecular size In addition, a technical limitation in the Q-Chem code prevents NICS values from being computed with the CAM-B3LYP functional. Furthermore, the self-interaction error of the standard B3LYP functional is considered negligible for benzene, due to its high degree of electron delocalization.

In choosing the basis set, diffuse functions were deliberately excluded to ensure that, during compression with GOSTSHYP, no electron density extends beyond the defined cavity, thereby avoiding potential sources of error.

2 Adjustment of van der Waals Radii

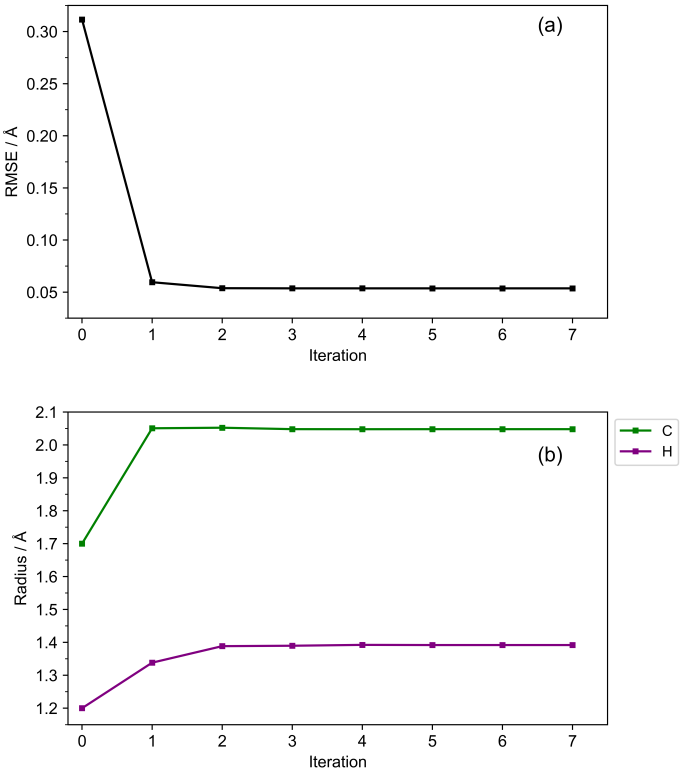

Figure S1: Changes in the RMSE (a) and van der Waals radii of carbon and hydrogen (b) during BFGS minimization. The optimized van der Waals radii were determined to be 2.0478 Å for carbon and 1.3919 Å for hydrogen (RMSE $<$ 0.054 Å).

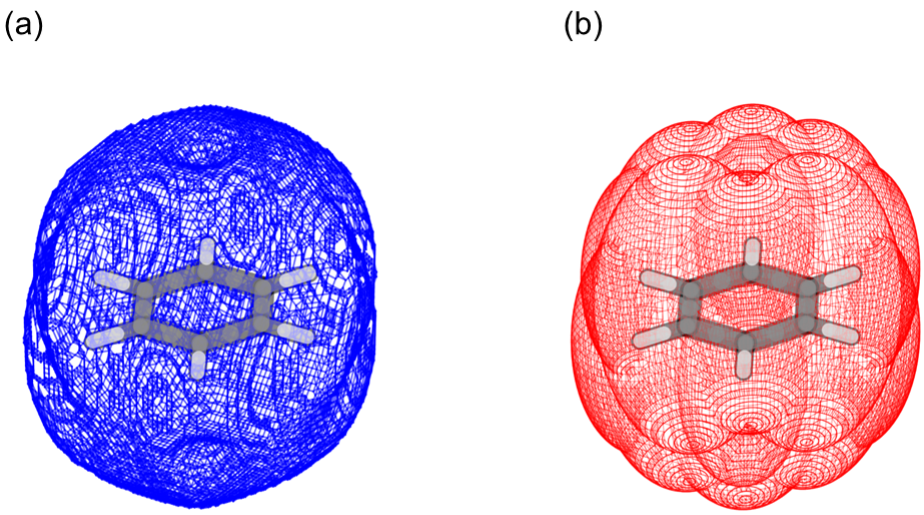

Figure S2: 0.001 e/bohr^3 isodensity surface (a) and adjusted cavity (b) of the benzene molecule.

3 Single Benzene Molecule in the Crystal

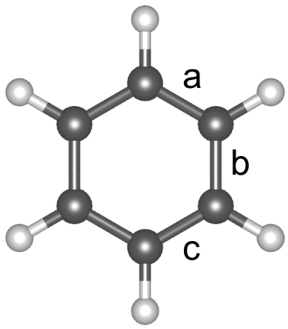

Figure S3: Asymmetrical benzene molecule in the crystal with unequal carbon carbon bond lengths a, b and c.

Table S1: Changes in the unequal bond lengths a, b and c of the asymmetric benzene molecule in the crystal

Pressure / GPa	a / Å	b / Å	c / Å
0	1.39345	1.39376	1.39366
5	1.38953	1.38949	1.38917
10	1.38539	1.38497	1.38459
15	1.38149	1.38090	1.38030
20	1.37785	1.37717	1.37619
25	1.37451	1.37353	1.37234
30	1.37142	1.37035	1.36888
35	1.36839	1.36711	1.36567
40	1.36552	1.36410	1.36255
45	1.36280	1.36137	1.35953
50	1.36023	1.35861	1.35677
55	1.35777	1.35609	1.35411
60	1.35530	1.35361	1.35161
65	1.35320	1.35125	1.34914
70	1.35092	1.34898	1.34675
75	1.34880	1.34678	1.34456
80	1.34670	1.34467	1.34246
85	1.34483	1.34265	1.34050
90	1.34302	1.34067	1.33860
95	1.34110	1.33878	1.33663
100	1.33928	1.33688	1.33484

4 BLA - Definition 2

$$\text{BLA (def 2)} = \left| \frac{R_2 + R_4 + R_6}{3} - \frac{R_1 + R_3 + R_5}{3} \right| \tag{1}$$

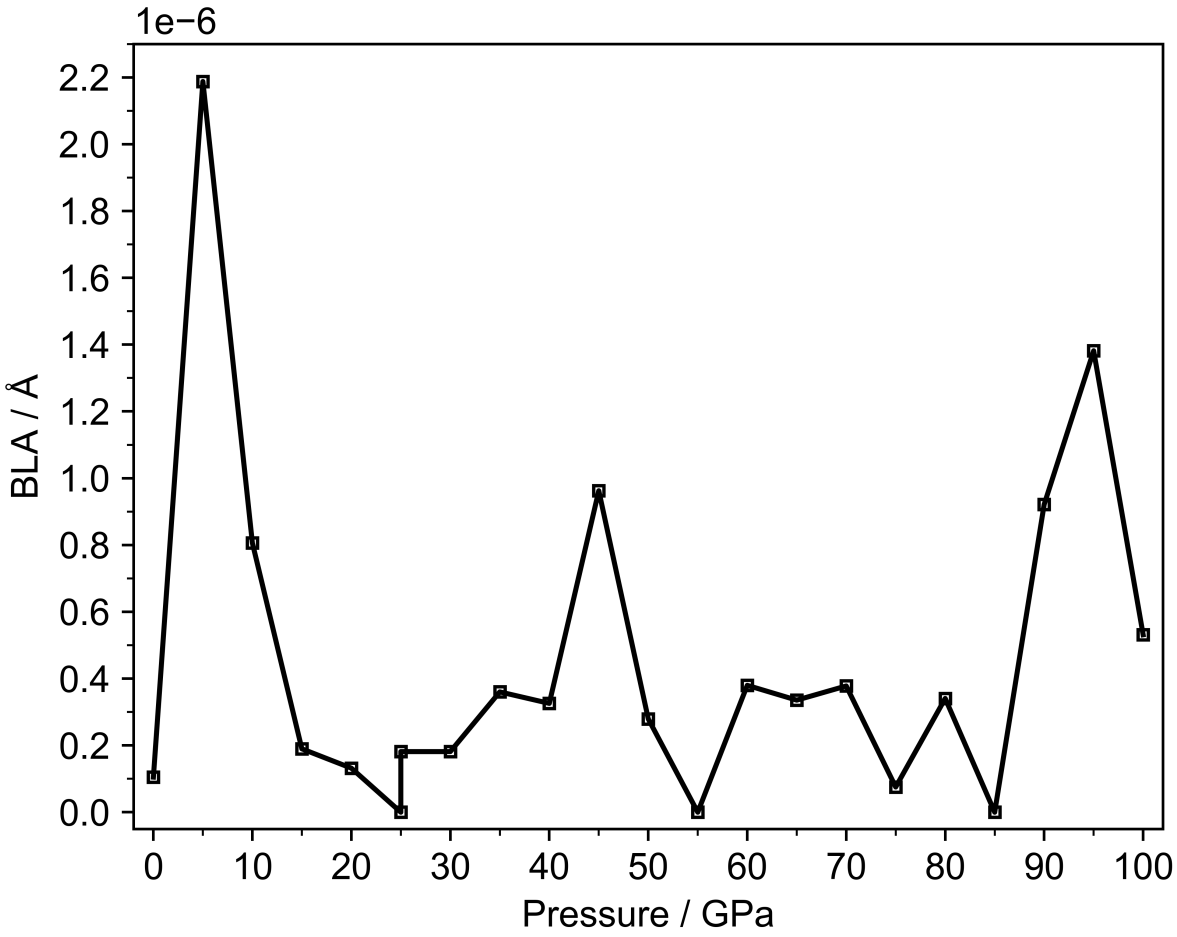

Figure S4: BLA index (def 2) for a single benzene molecule in the crystal lattice from 0 to 100 GPa.

5 Average Difference of C-C Bond Lengths Within the Benzene Ring

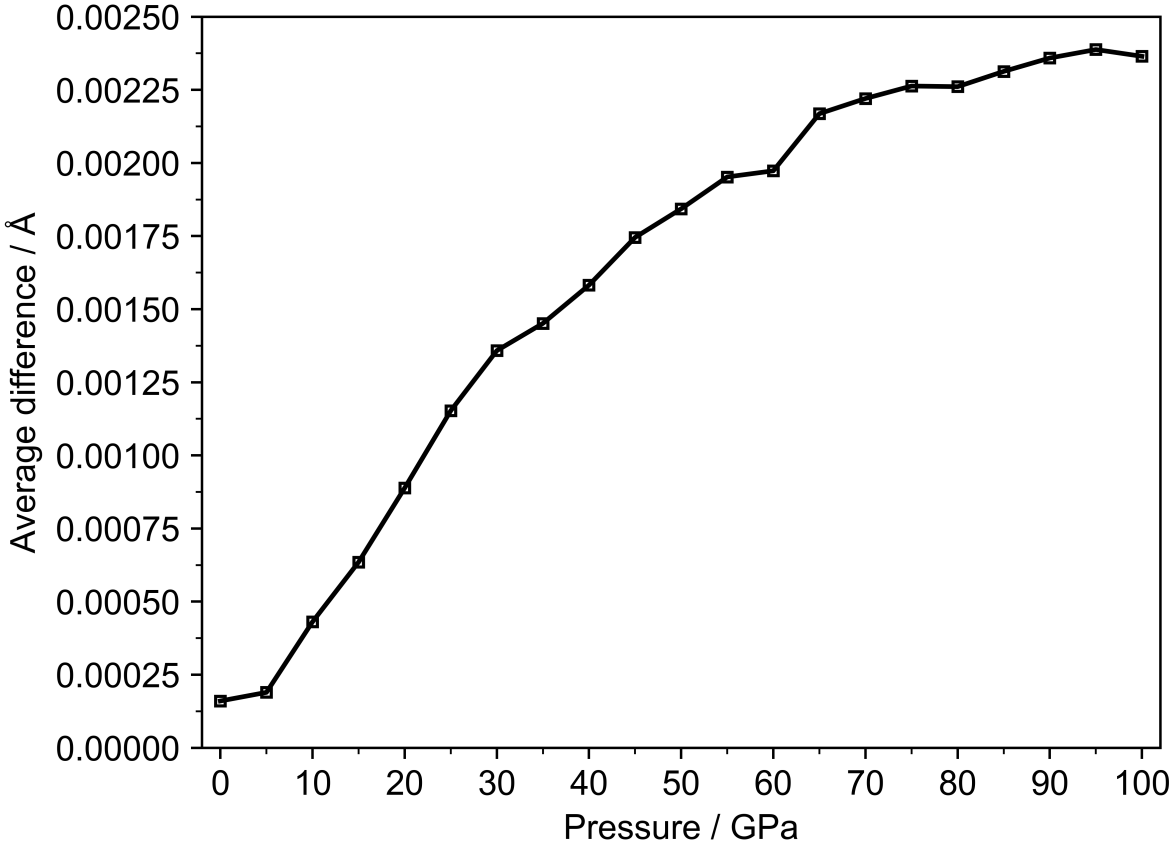

Figure S5: Average difference of the C–C bond lengths within the single benzene molecule in the crystal lattice from 0 to 100 GPa. The differences between all six bond lengths were considered, resulting in a total of 15 possible combinations.

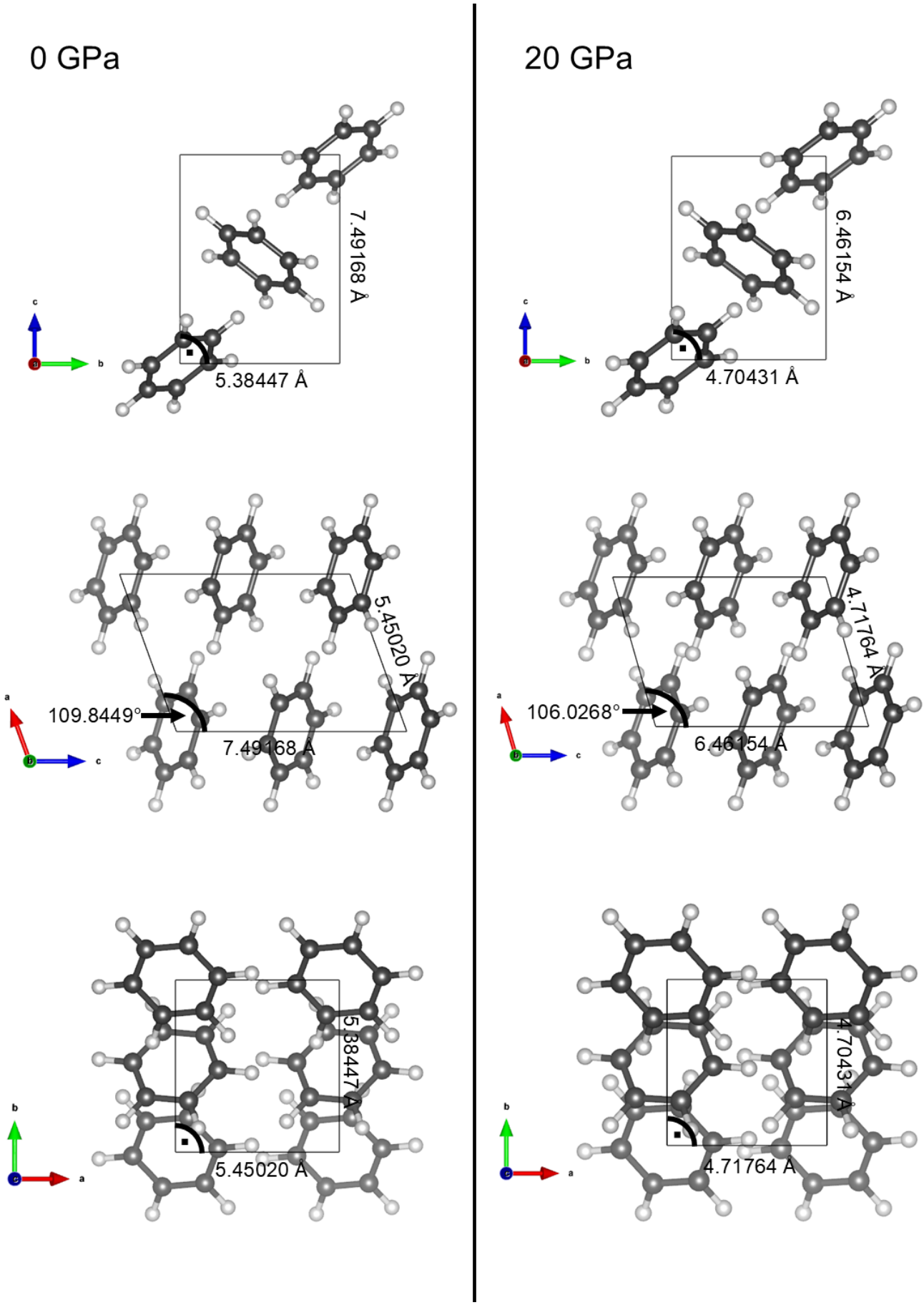

Figure S6: Unit cells of the benzene crystal structure in all three directions at 0 and 20 GPa with the corresponding cell parameters.

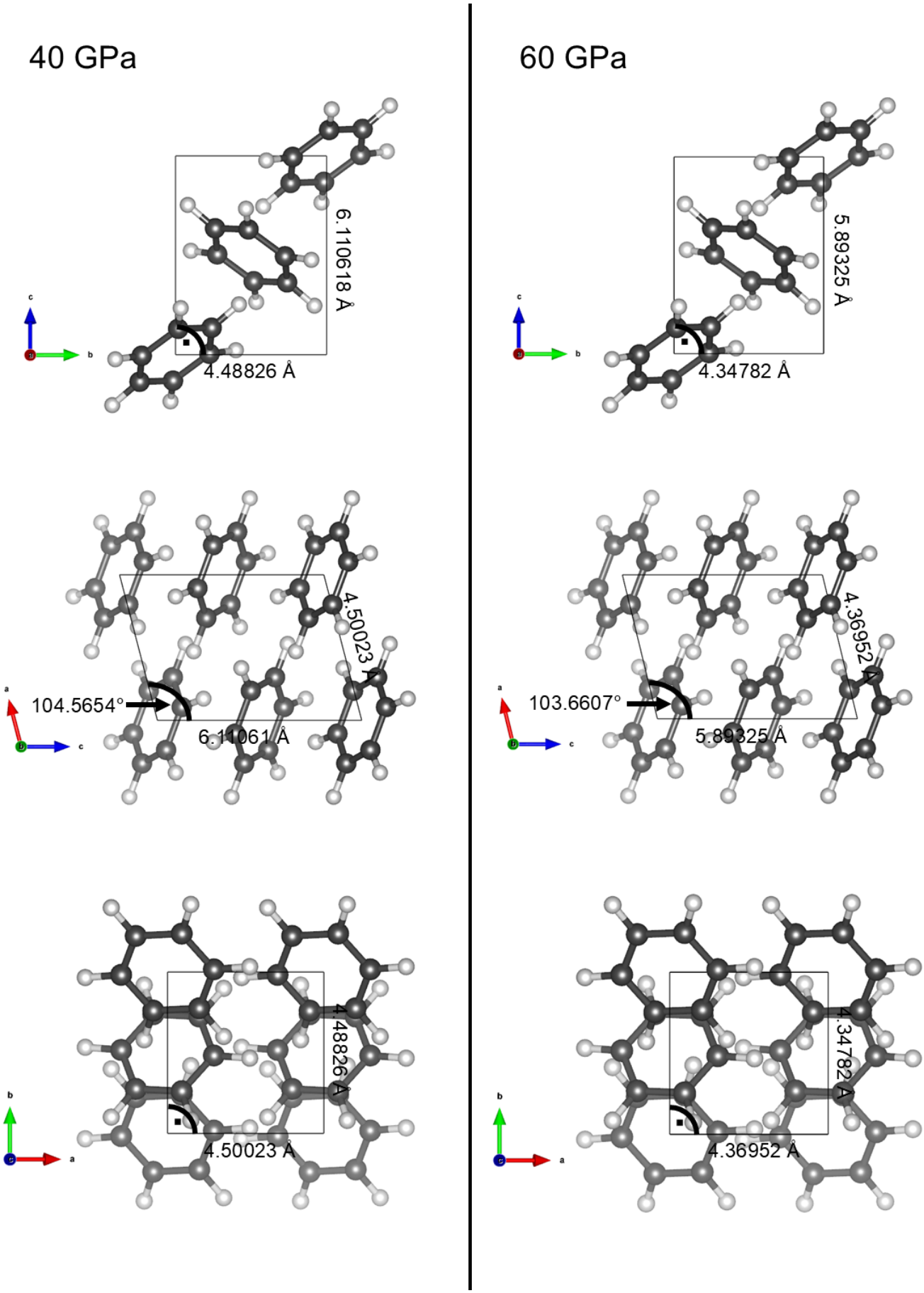

Figure S7: Unit cells of the benzene crystal structure in all three directions at 40 and 60 GPa with the corresponding cell parameters.

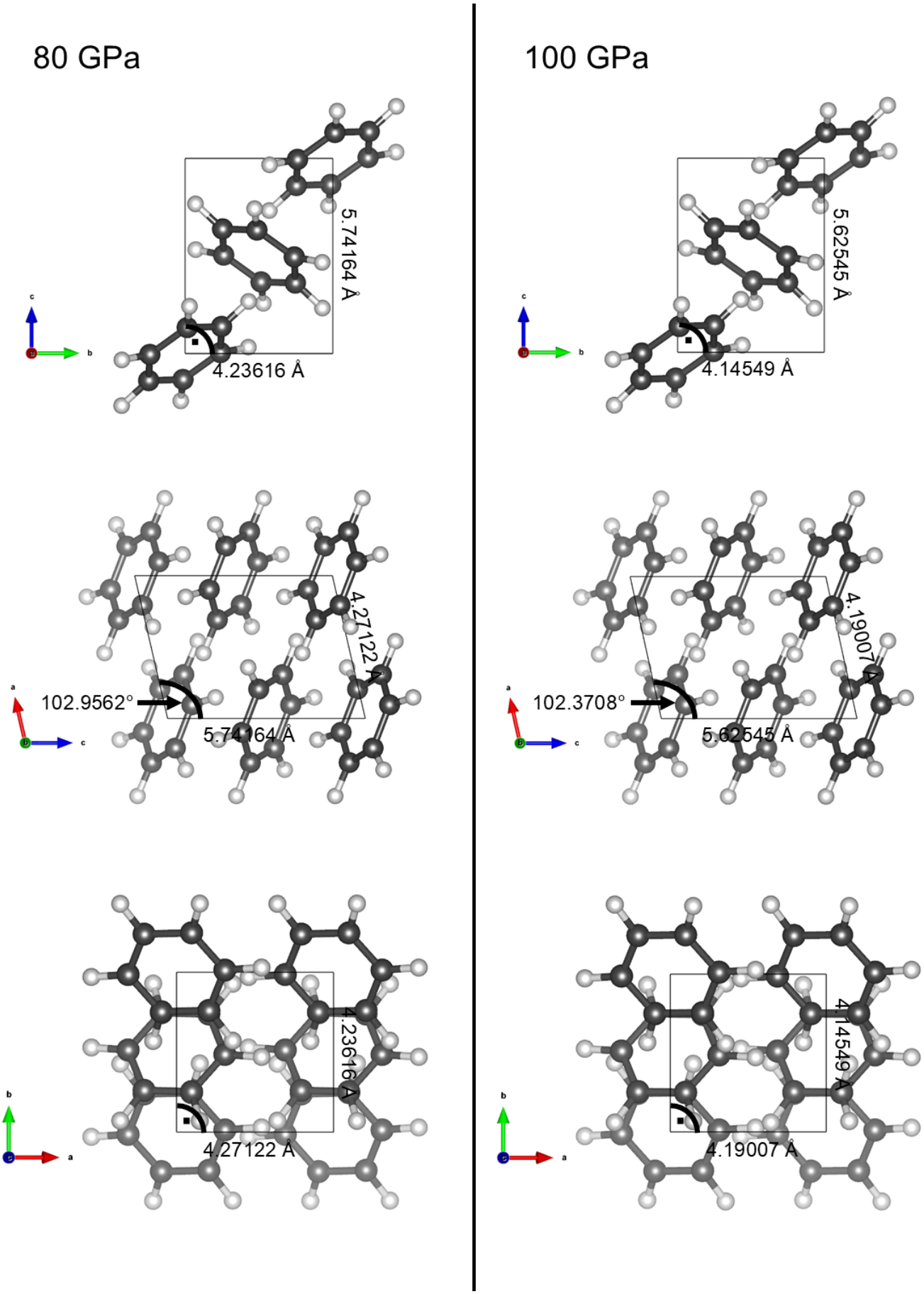

Figure S8: Unit cells of the benzene crystal structure in all three directions at 80 and 100 GPa with the corresponding cell parameters.

6 HOMA - Reparameterization under Pressure

$$\mathrm{HOMA} = 1 - \frac{\alpha}{\mathrm{n}} \sum_{\mathrm{i}=1}^{\mathrm{n}} (\mathrm{R_i} - \mathrm{R_{ref}})^2 \tag{2}$$

$$\mathrm{R_{ref}} = \frac{(\mathrm{R_s} + 2\mathrm{R_d})}{3} \tag{3}$$

$$\alpha = \frac{2}{(\mathrm{R_s} - \mathrm{R_{ref}})^2 + (\mathrm{R_d} - \mathrm{R_{ref}})^2} \tag{4}$$

Table S2: Bond lengths of the central carbon-carbon single and double bonds of ethane and ethene as reference systems under pressure. The optimizations were performed with GOSTSHYP at the B3LYP-D3/cc-pVTZ level of theory.

Pressure / GPa	C-C bond length (ethane) / Å	C=C bond length (ethene) / Å
0	1.52847	1.32447
5	1.52368	1.32178
10	1.51914	1.31917
15	1.51482	1.31661
20	1.51068	1.31408
25	1.50620	1.31159
30	1.50234	1.30914
35	1.49864	1.30673
40	1.49501	1.30436
45	1.49159	1.30188
50	1.48830	1.29955
55	1.48513	1.29725
60	1.48206	1.29499
65	1.47911	1.29280
70	1.47625	1.29062
75	1.47348	1.28847
80	1.47080	1.28636
85	1.46819	1.28428
90	1.46567	1.28224
95	1.46321	1.28024
100	1.46082	1.27827

Table S3: Bond lengths of the carbon-carbon single and double bonds of butadiene as reference system under pressure. The optimizations were performed with GOSTSHYP at the B3LYP-D3/cc-pVTZ level of theory.

Pressure / GPa	C-C bond length / Å	C=C bond length / Å
0	1.45351	1.33416
5	1.44916	1.33182
10	1.44484	1.32937
15	1.44067	1.32676
20	1.43670	1.32458
25	1.43301	1.32206
30	1.42941	1.31977
35	1.42594	1.31752
40	1.42267	1.31530
45	1.41936	1.31314
50	1.41622	1.31098
55	1.41319	1.30888
60	1.41026	1.30683
65	1.40742	1.30481
70	1.40466	1.30282
75	1.40197	1.30087
80	1.39936	1.29896
85	1.39682	1.29708
90	1.39435	1.29523
95	1.39194	1.29341
100	1.38959	1.29163

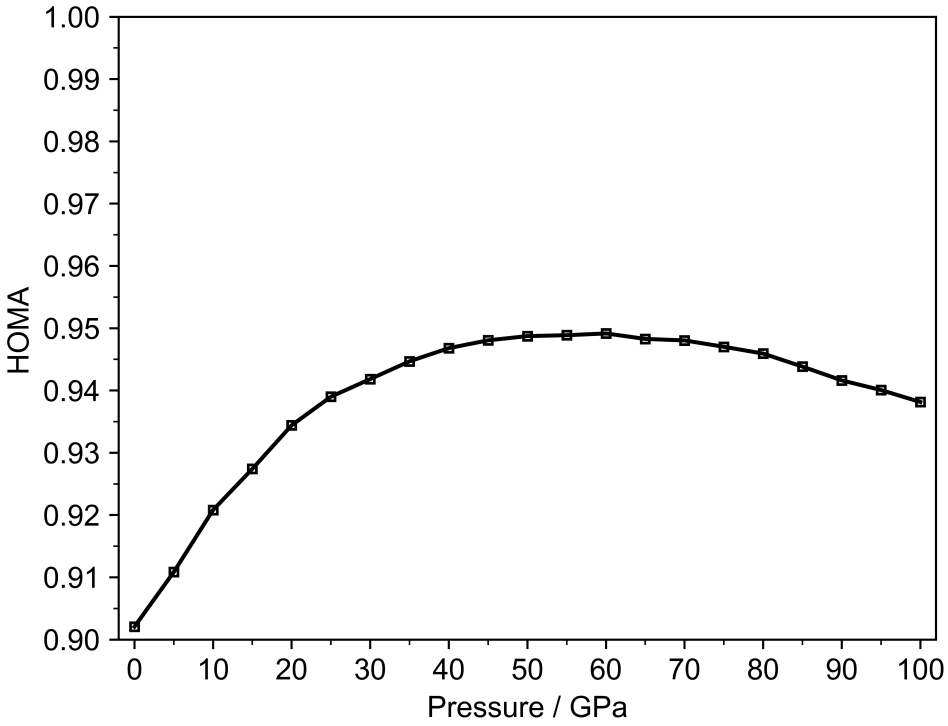

Figure S9: HOMA index using butadiene as reference system for a single benzene molecule in the crystal lattice from 0 to 100 GPa.

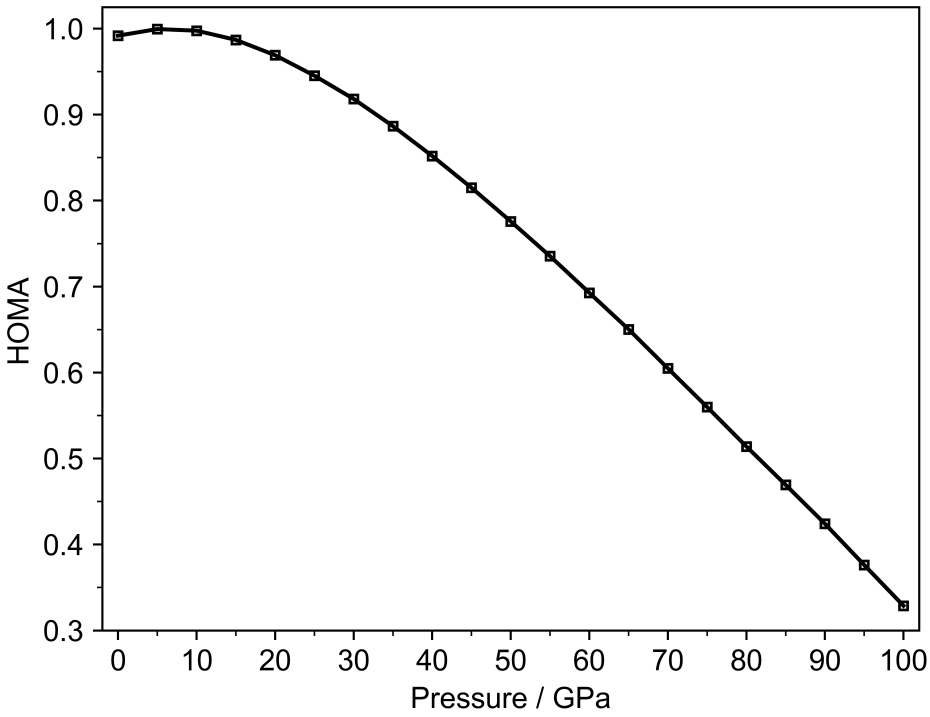

Figure S10: HOMA index using the standard parameters (R_{ref} = 1.388 Å, α = 257.7) for a single benzene molecule in the crystal lattice from 0 to 100 GPa.[43]

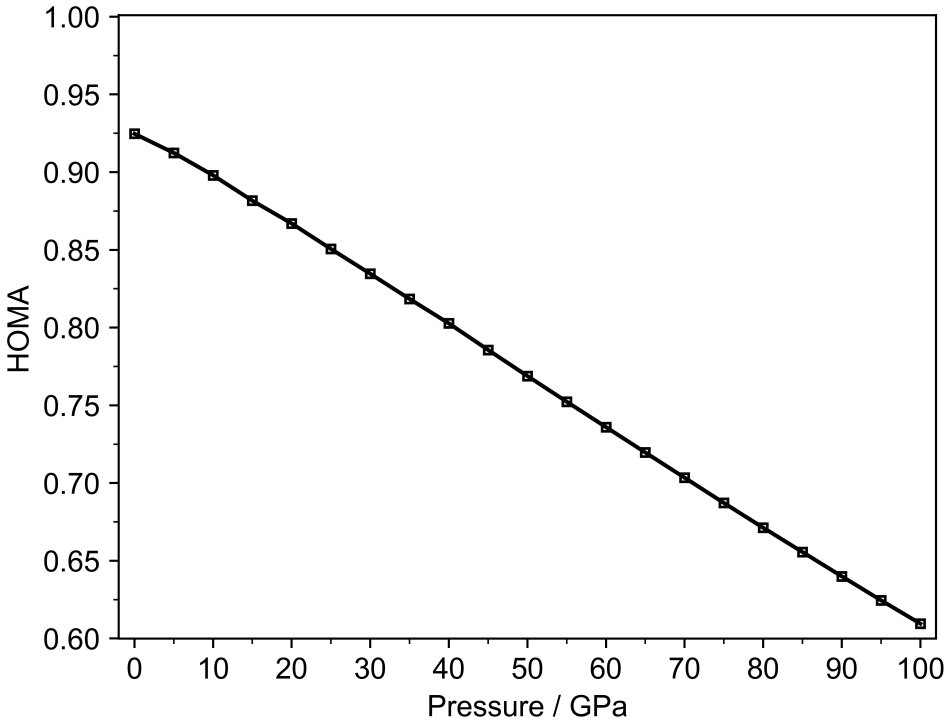

Figure S11: HOMA index using butadiene as reference system for a single benzene molecule from 0 to 100 GPa. The optimizations were performed with GOSTSHYP at the B3LYP-D3/cc-pVTZ level of theory.

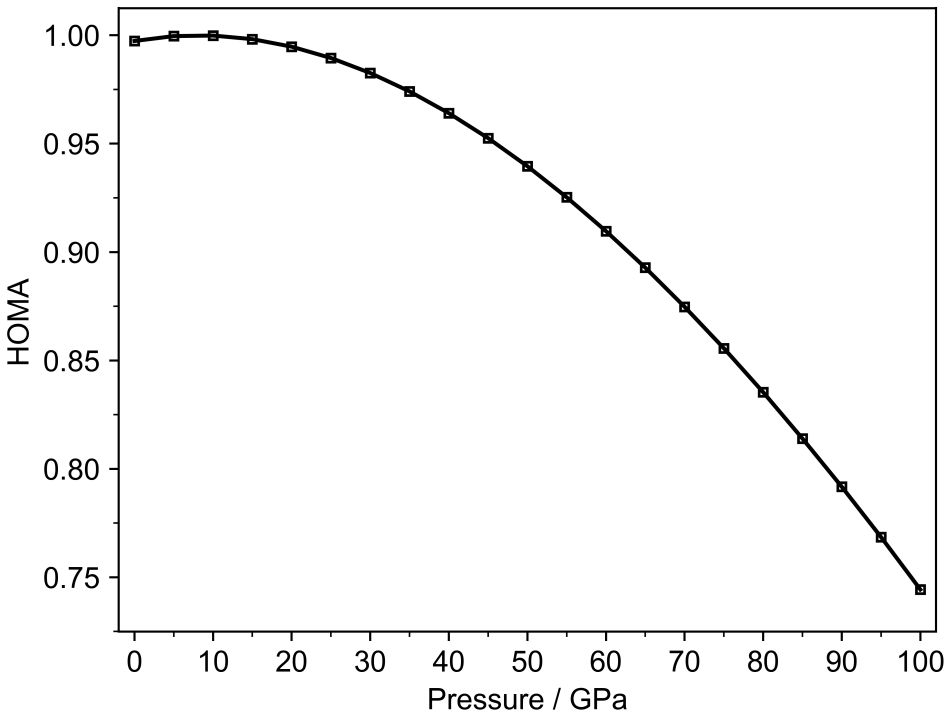

Figure S12: HOMA index using the standard parameters (R_{ref} = 1.388 Å, α = 257.7) for a single benzene molecule from 0 to 100 GPa.[43] The optimizations were performed with GOSTSHYP at the B3LYP-D3/cc-pVTZ level of theory.

Table S4: Bond lengths of the central carbon-carbon single and double bonds of ethane and ethene as reference systems under pressure. The optimizations were performed with GOSTSHYP at the CAM-B3LYP-D3/cc-pVTZ level of theory.

Pressure / GPa	C-C bond length (ethane) / Å	C=C bond length (ethene) / Å
0	1.52143	1.31873
20	1.50428	1.30872
40	1.48942	1.29929
60	1.47686	1.29015
80	1.46596	1.28174
100	1.45628	1.27381

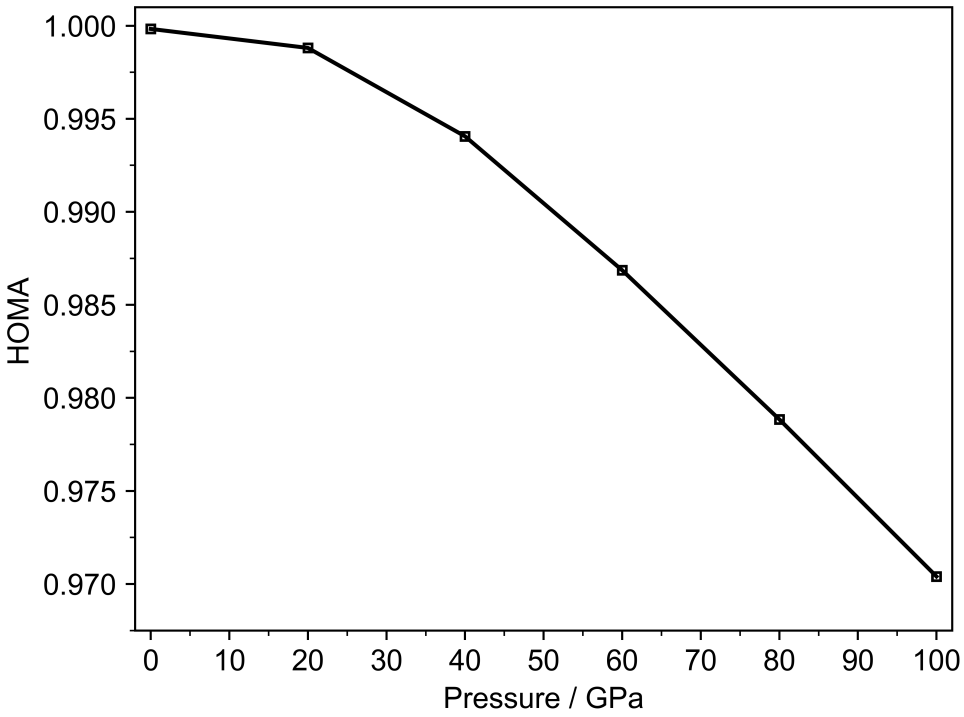

Figure S13: HOMA index using ethane and ethene as reference systems for a single benzene molecule from 0 to 100 GPa. The optimizations were performed with GOSTSHYP at the CAM-B3LYP-D3/cc-pVTZ level of theory.

Table S5: Bond lengths of the central carbon-carbon single and double bonds of butadiene as reference system under pressure. The optimizations were performed with GOSTSHYP at the CAM-B3LYP-D3/cc-pVTZ level of theory.

Pressure / GPa	C-C bond length / Å	C=C bond length / Å
0	1.45430	1.32600
20	1.43790	1.31665
40	1.42401	1.30792
60	1.41192	1.29976
80	1.40120	1.29215
100	1.39156	1.28503

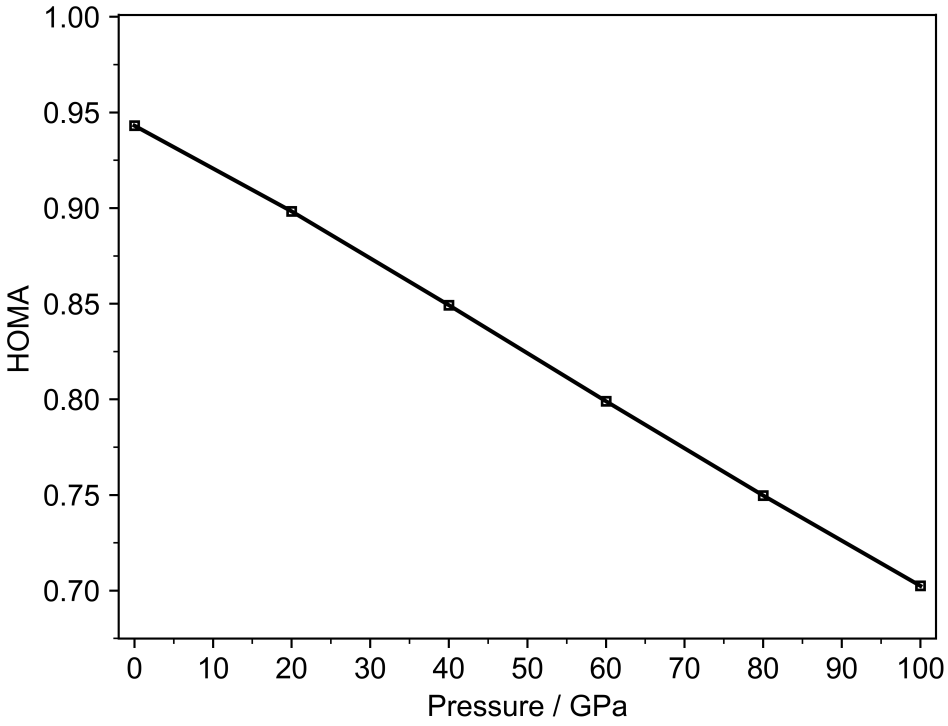

Figure S14: HOMA index using butadiene as reference system for a single benzene molecule from 0 to 100 GPa. The optimizations were performed with GOSTSHYP at the CAM-B3LYP-D3/cc-pVTZ level of theory.

7 Linear Response Function

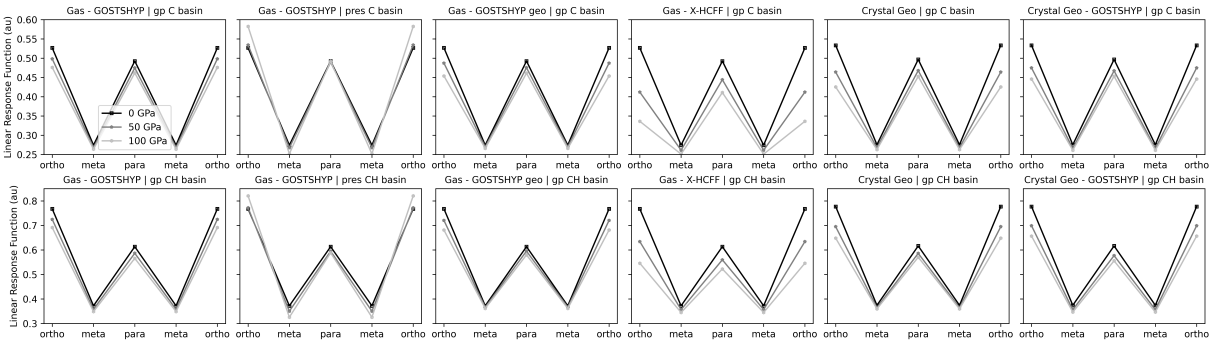

Figure S15: Condensed linear response function in the independent particle approximation and Hirshfeld space partition. Values are provided at 0, 50 and 100 GPa along the ring atoms (ortho-meta-para-meta-ortho). The top row displays the regions of the carbon atoms, while the bottom row takes the carbon and hydrogen atoms together. The Bondi set of radii were used in the pressure models. The considered pressure models were an isolated molecule with the X-HCFF model (Gas - X-HCFF), an isolated molecule with the GOSTSHYP model (Gas - GOSTSHYP), a gas phase single point calculation on the geometry of the GOSTSHYP model (Gas - GOSTSHYP Geo) and a GOSTSHYP calculation on the geometry extracted from the benzene crystal (Crystal Geo - GOSTSHYP). Additionally, pressurized atomic densities were tested for the GOSTSHYP model.

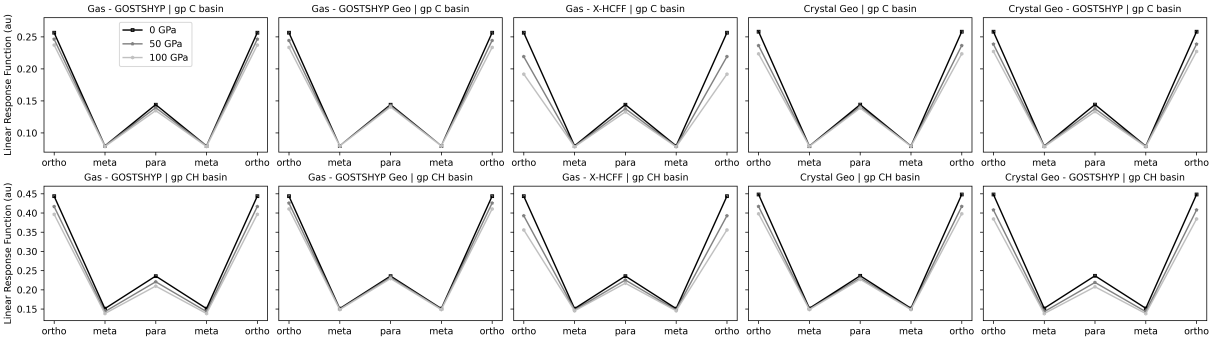

Figure S16: Condensed linear response function in the local density approximation and Hirshfeld space partition. Values are provided at 0, 50 and 100 GPa along the ring atoms (ortho-meta-para-meta-ortho). The top row displays the regions of the carbon atoms, while the bottom row takes the carbon and hydrogen atoms together. The Bondi set of radii were used in the pressure models. The considered pressure models were an isolated molecule with the X-HCFF model (Gas - X-HCFF), an isolated molecule with the GOSTSHYP model (Gas - GOSTSHYP), a gas phase single point calculation on the geometry of the GOSTSHYP model (Gas - GOSTSHYP Geo) and a GOSTSHYP calculation on the geometry extracted from the benzene crystal (Crystal Geo - GOSTSHYP). Additionally, pressurized atomic densities were tested for the GOSTSHYP model.

8 Delocalization Indices

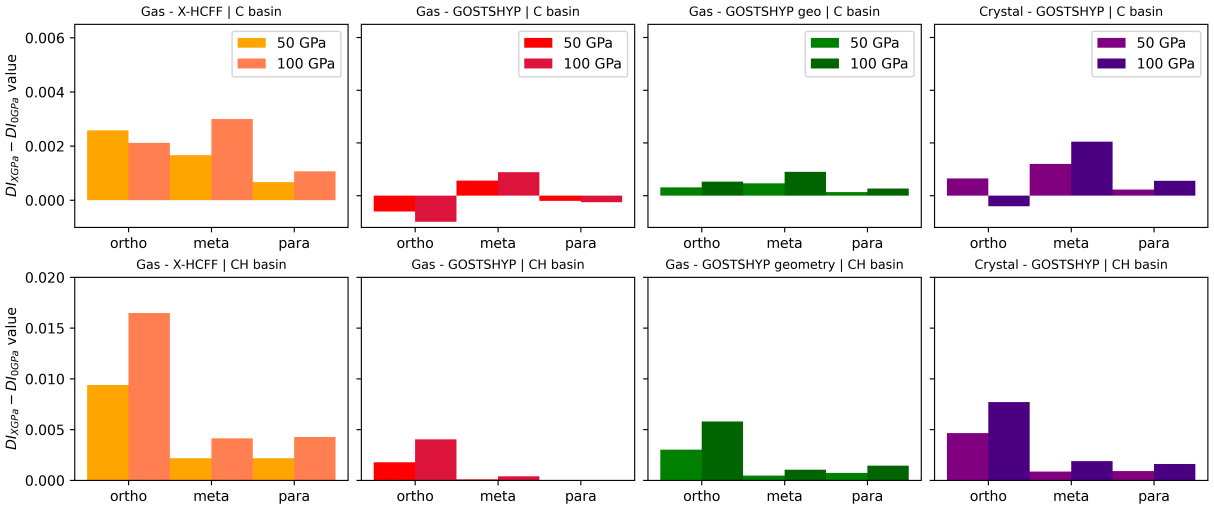

Figure S17: Change in delocalization indices for ortho, meta and para related carbon atoms using the QTAIM basins when going from 0 to 50 and 0 to 100 GPa. The top row displays the regions of the carbon atoms, while the bottom row takes the carbon and hydrogen atoms together. The radii used in the pressure model were those fitted to the 0.001 e/bohr3 isosurface. The considered pressure models were an isolated molecule with the X-HCFF model (Gas - X-HCFF), an isolated molecule with the GOSTSHYP model (Gas - GOSTSHYP), a gas phase single point calculation on the geometry of the GOSTSHYP model (Gas - GOSTSHYP Geo) and a GOSTSHYP calculation on the geometry extracted from the benzene crsytal (Crystal Geo - GOSTSHYP).

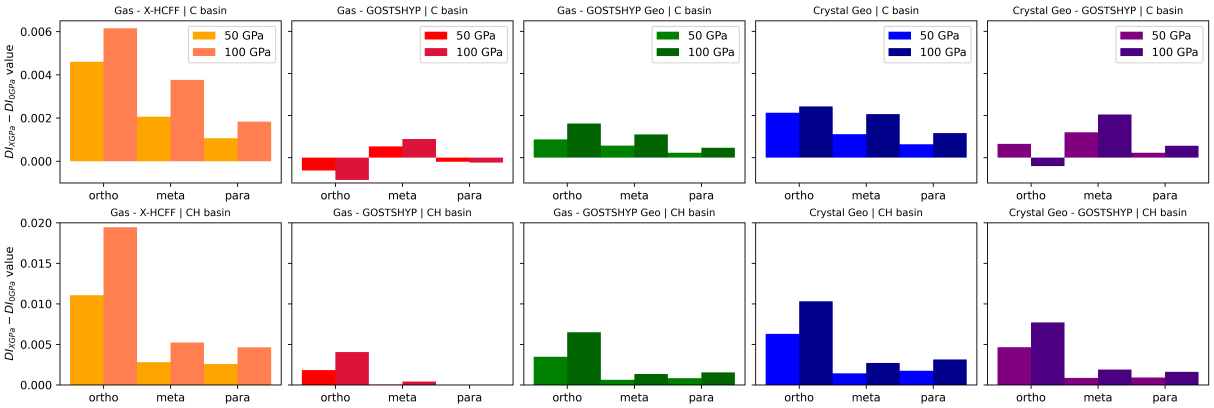

Figure S18: Change in delocalization indices for ortho, meta and para related carbon atoms using the QTAIM basins when going from 0 to 50 and 0 to 100 GPa. The top row displays the regions of the carbon atoms, while the bottom row takes the carbon and hydrogen atoms together. The radii used in the pressure model were the standard Bondi radii with a scaling factor of 1.3. The considered pressure models were an isolated molecule with the X-HCFF model (Gas - X-HCFF), an isolated molecule with the GOSTSHYP model (Gas - GOSTSHYP), a gas phase single point calculation on the geometry of the GOSTSHYP model (Gas - GOSTSHYP Geo), a gas phase single point calculation on the geometry extracted from the benzene crystal under pressure (Crystal Geo) and a GOSTSHYP calculation on the geometry extracted from the benzene crsytal (Crystal Geo - GOSTSHYP).

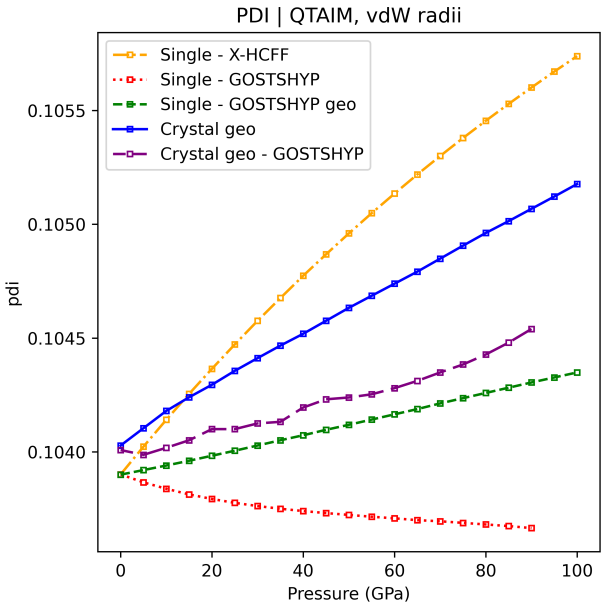

Figure S19: *Para*-delocalization index as a function of pressure for benzene. The radii used in the pressure model were the standard Bondi radii with a scaling factor of 1.3. The considered pressure models were an isolated molecule with the X-HCFF model (Gas - X-HCFF), an isolated molecule with the GOSTSHYP model (Gas - GOSTSHYP), a gas phase single point calculation on the geometry of the GOSTSHYP model (Gas - GOSTSHYP Geo), a gas phase single point calculation on the geometry extracted from the benzene crystal under pressure (Crystal Geo) and a GOSTSHYP calculation on the geometry extracted from the benzene crsytal (Crystal Geo - GOSTSHYP).

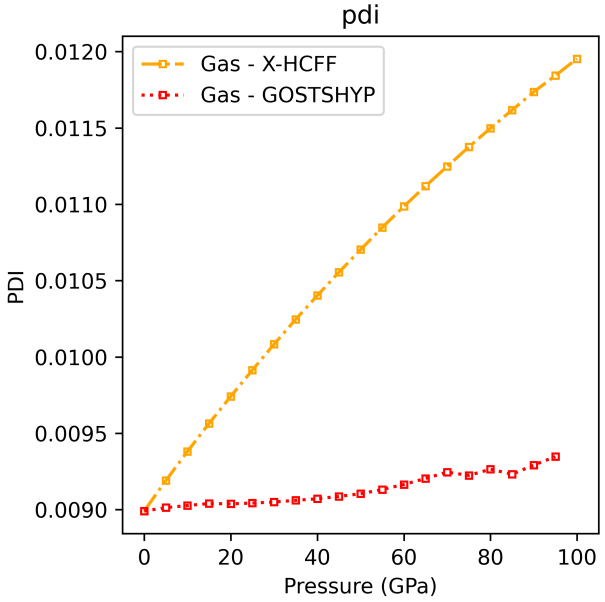

Figure S20: *Para*-delocalization index as a function of pressure for cyclohexane. The radii used in the pressure model were the standard Bondi radii with a scaling factor of 1.3. The considered pressure models were an isolated molecule with the X-HCFF model (Gas - X-HCFF) and an isolated molecule with the GOSTSHYP model (Gas - GOSTSHYP).

9 Multicenter Indices

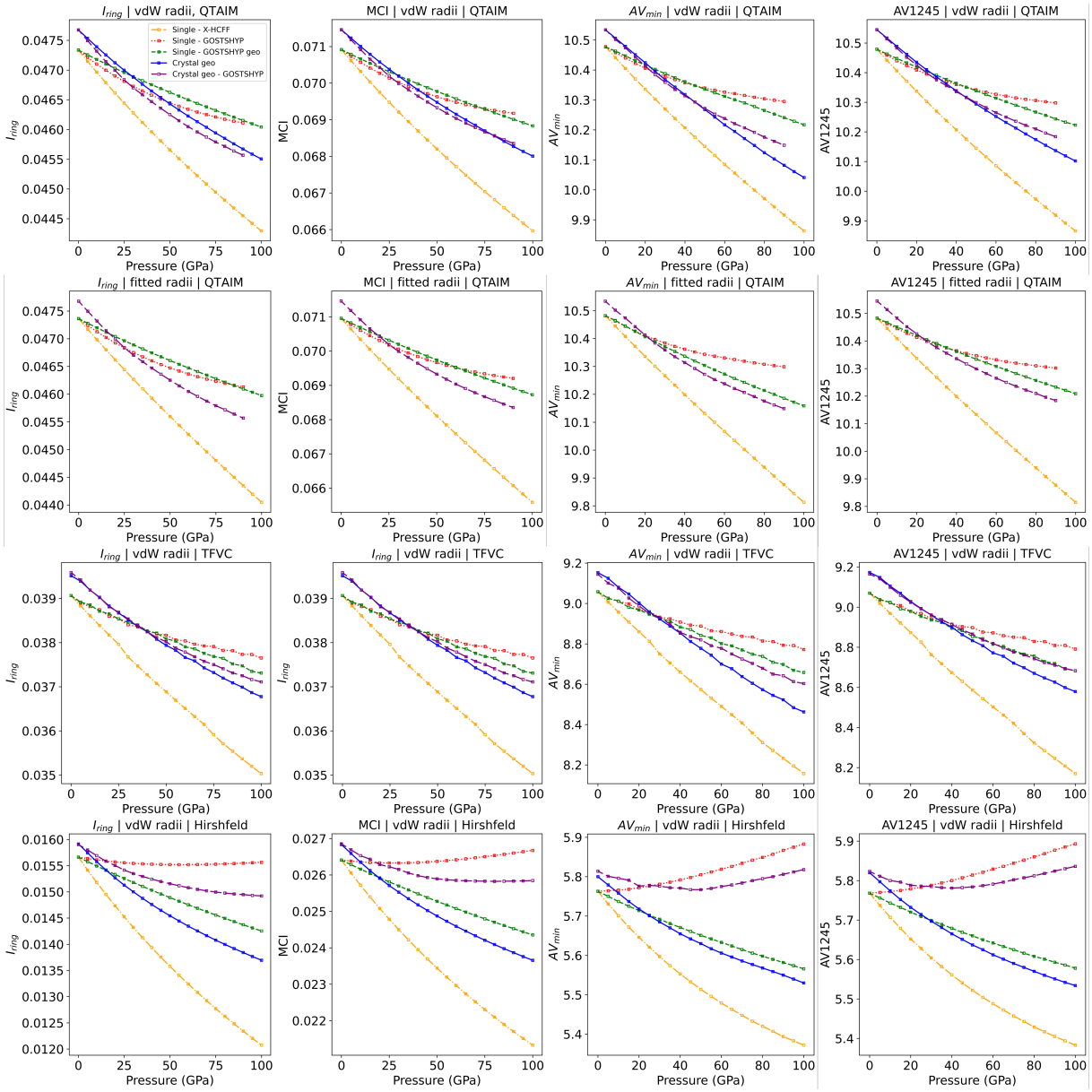

Figure S21: Multicenter Indices for different pressure models, partitions and radii types from 0 to 100 GPa. The considered pressure models were an isolated molecule with the X-HCFF model (Gas - X-HCFF), an isolated molecule with the GOSTSHYP model (Gas - GOSTSHYP), a gas phase single point calculation on the geometry of the GOSTSHYP model (Gas - GOSTSHYP Geo) and a GOSTSHYP calculation on the geometry extracted from the benzene crystal (Crystal Geo - GOSTSHYP). The QTAIM, TFVC and Hirshfeld partitions were considered. For the QTAIM partition, both the set of Bondi van der Waals radii and isosurface fitted radii were used in the pressure models.

10 Infinitely-thin Conducting Line Of Current Models.

The following plots show the data and model fits for the different pressure and ICLOC models with distinct fitting strategies. The data and models are provided for 0 and 20 GPa, on the basis of which the quality of the fit was visually assessed. The RMSE of the 0 GPa model is provided and the number of successful fits of the model (ranging from 0 to 6).

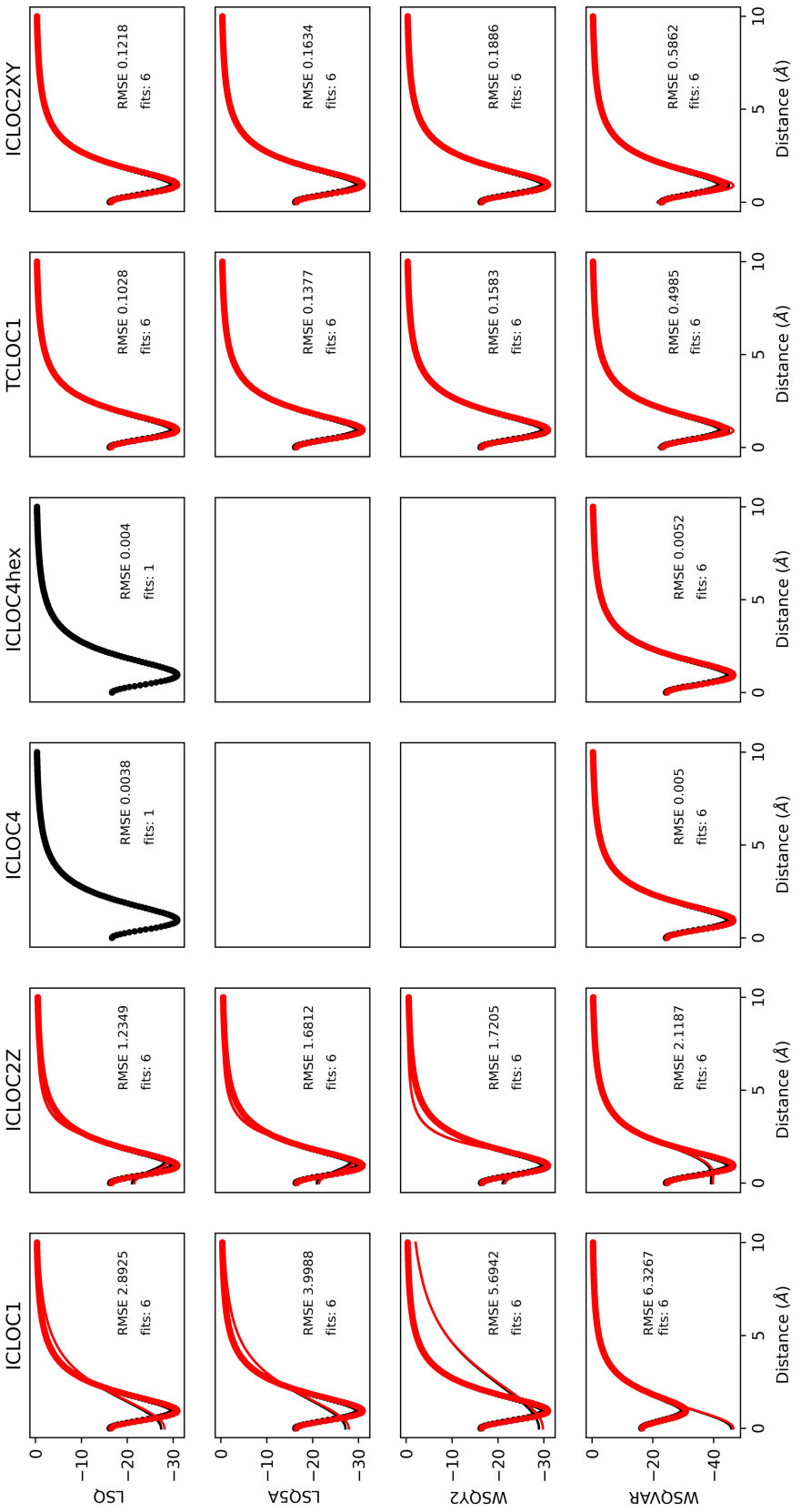

Figure S22: ICLOC fits for the XHCFF model.

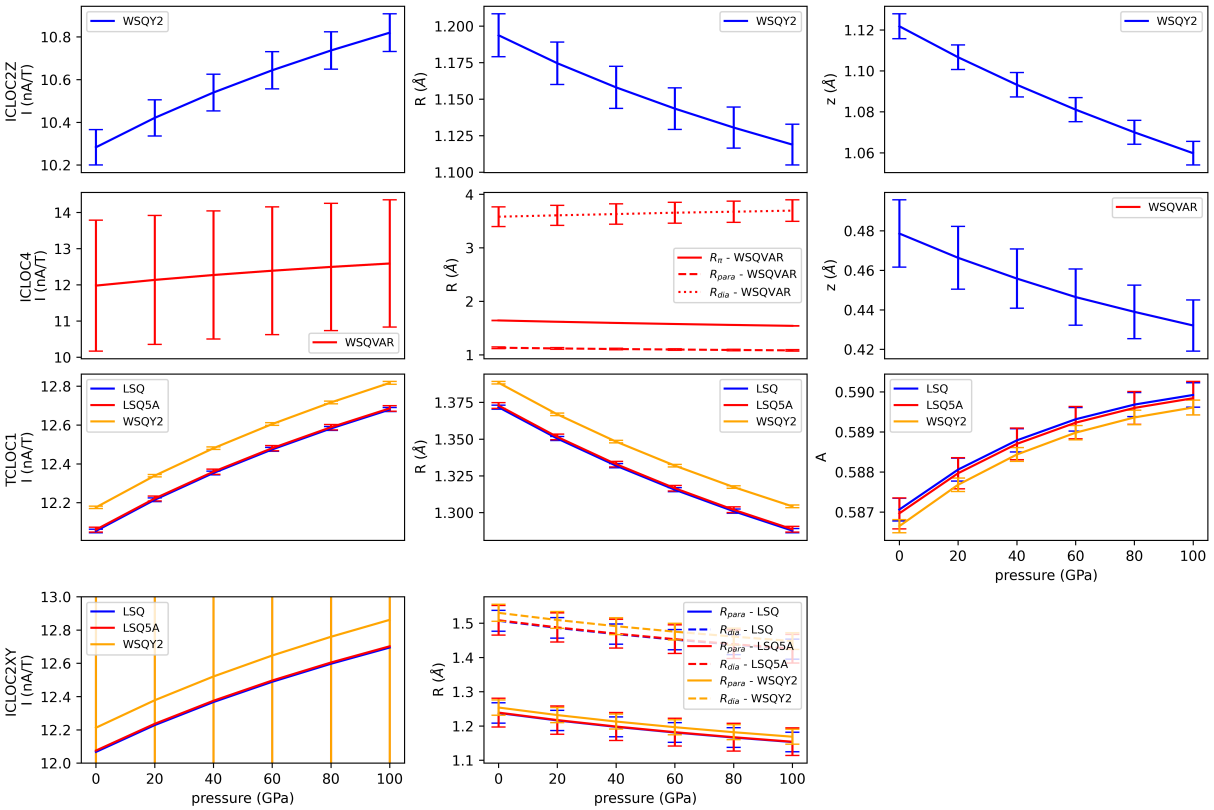

Figure S23: ICLOC parameters for the XHCFF model.

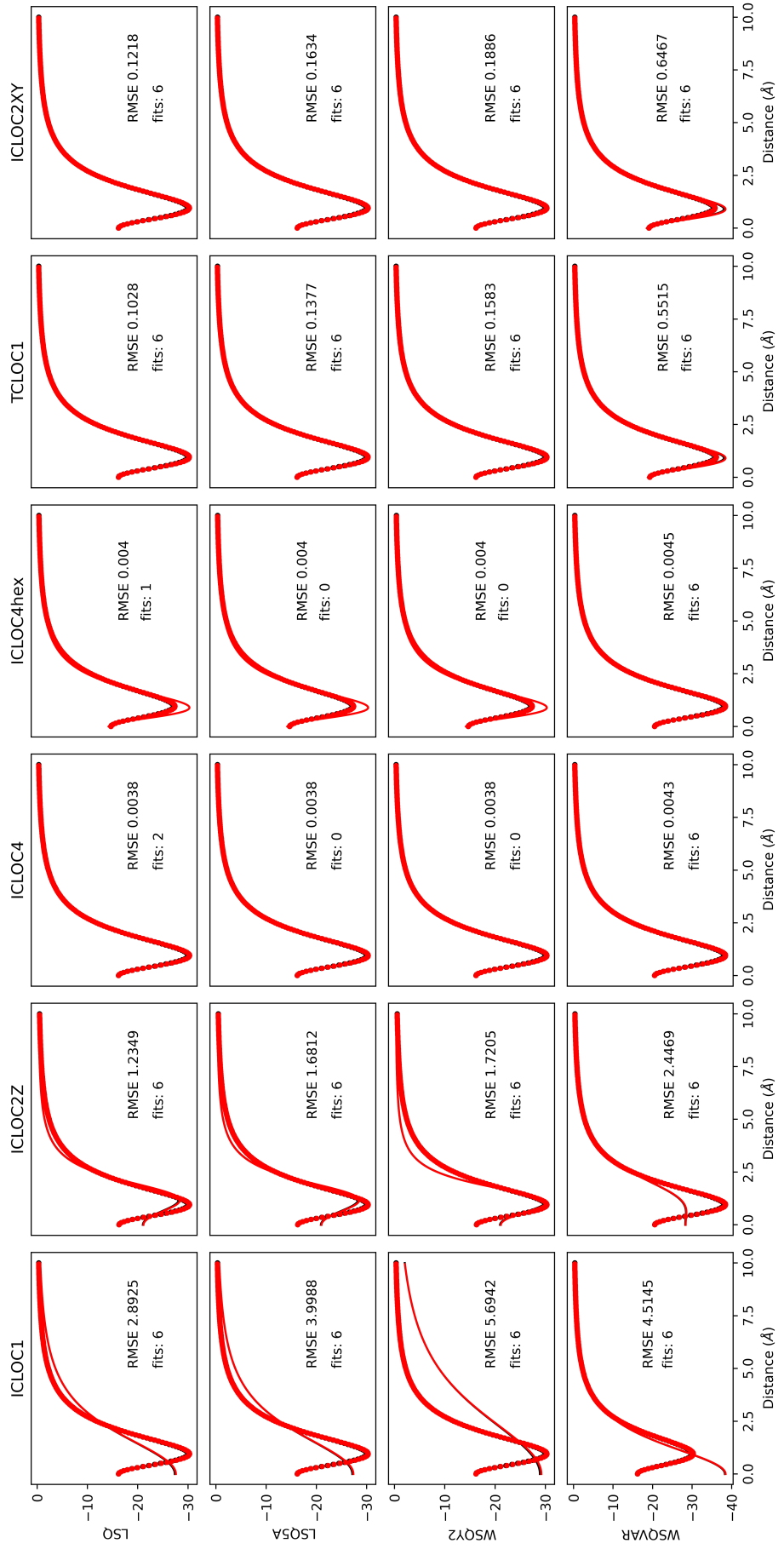

Figure S24: ICLOC fits for the GOSTSHYP geometry and gas phase electronic structure.

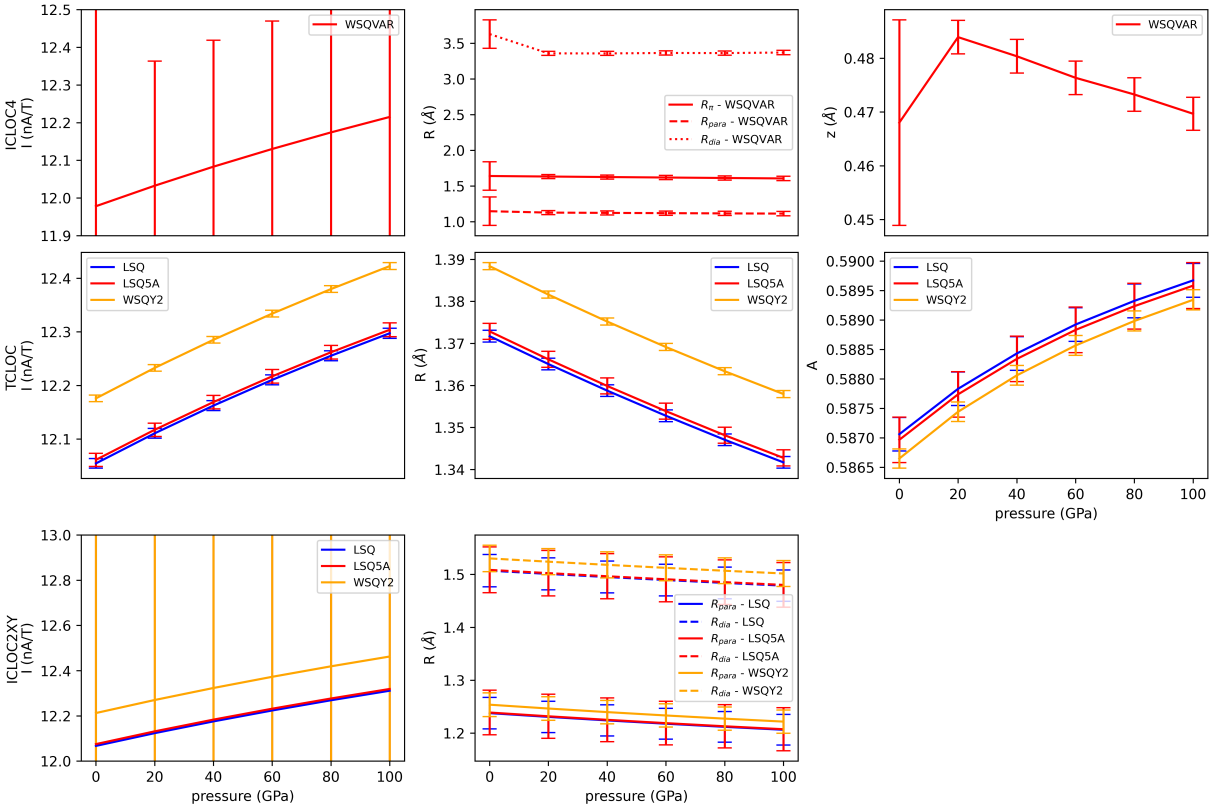

Figure S25: ICLOC parameters for the GOSTSHYP geometry and gas phase electronic structure.

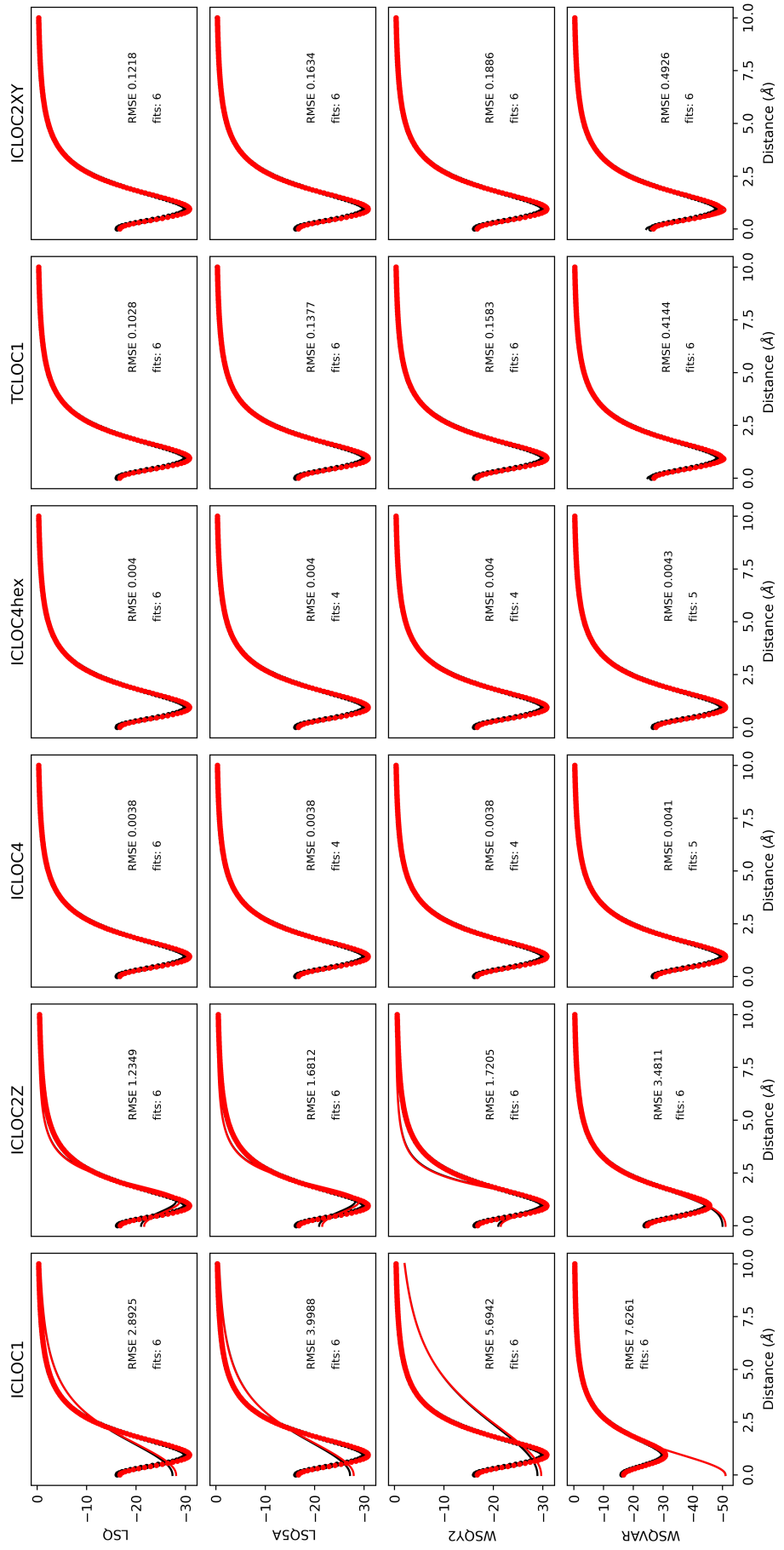

Figure S26: ICLOC fits for the GOSTSHYP model.

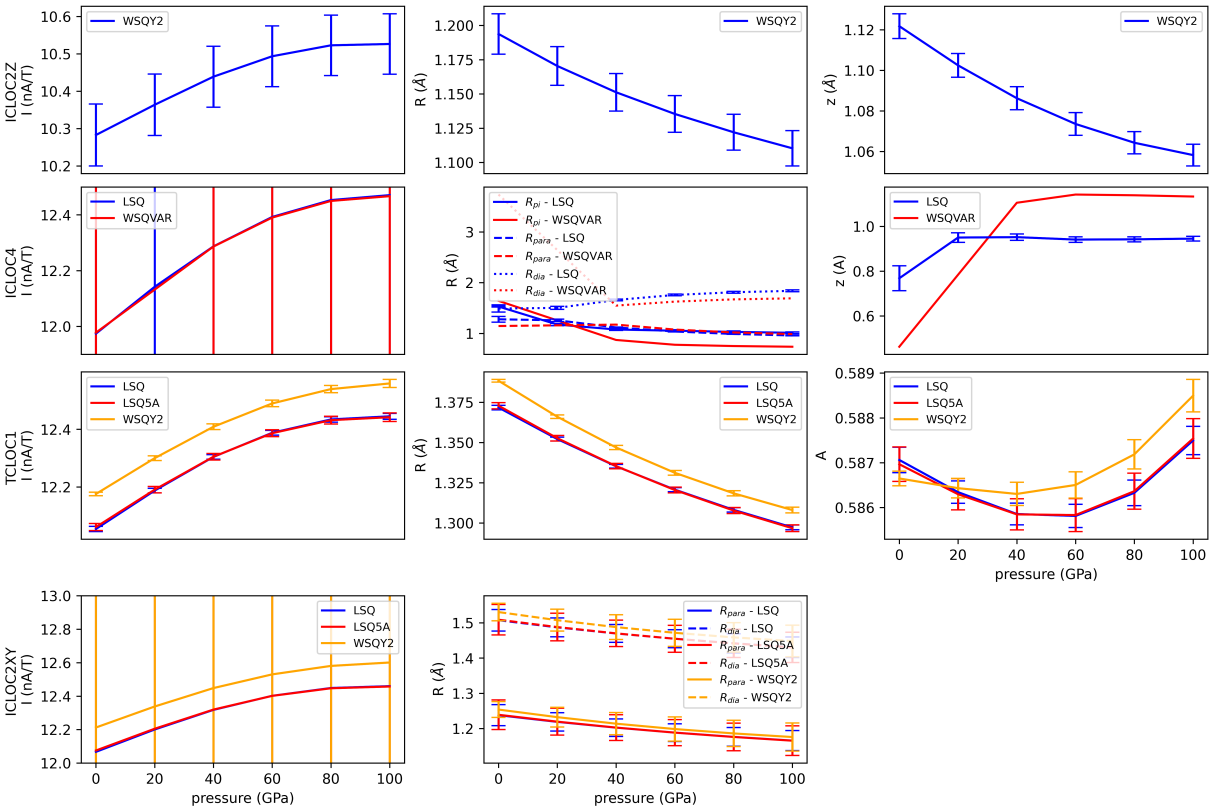

Figure S27: ICLOC parameters for the GOSTSHYP model.

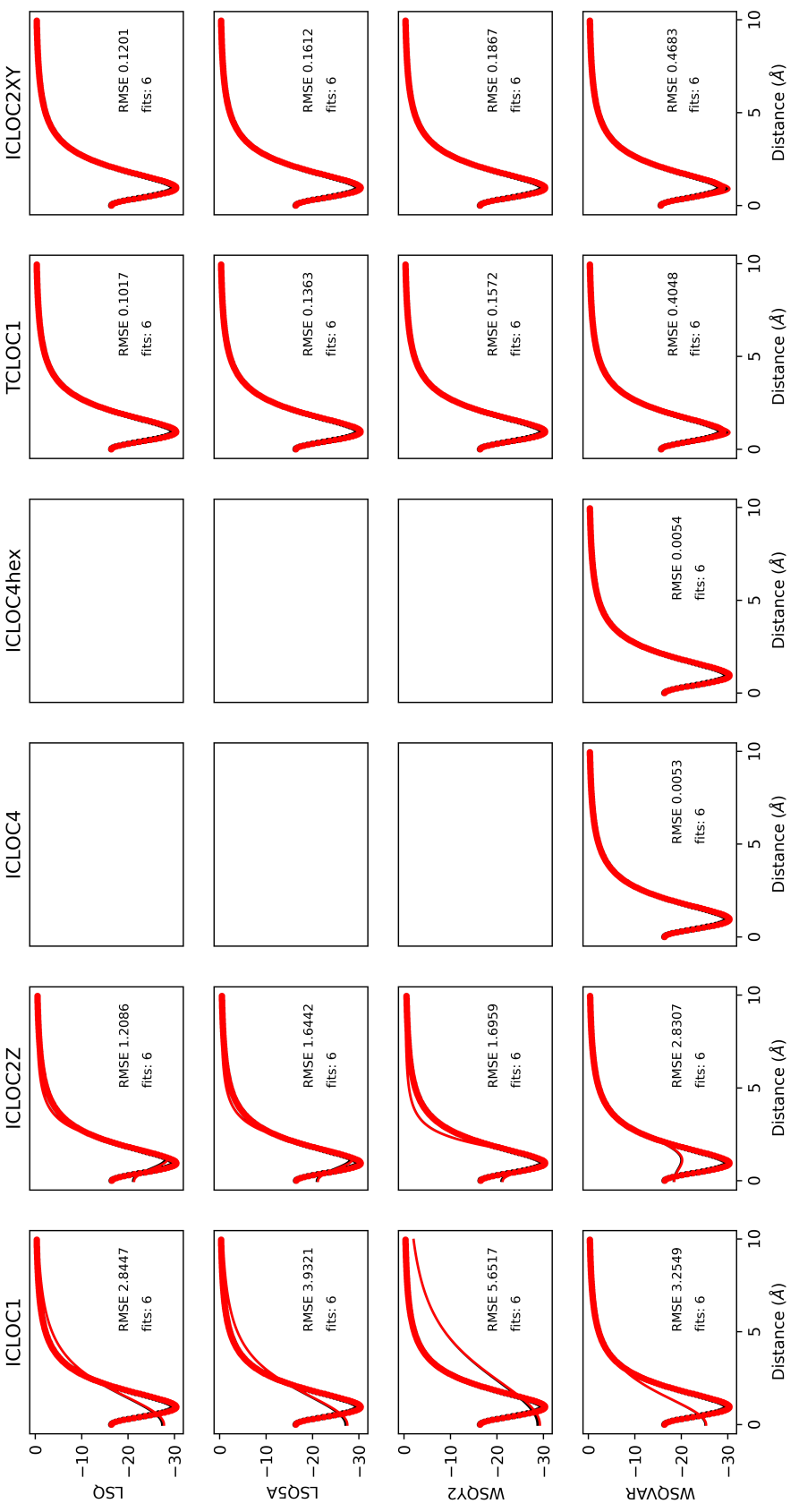

Figure S28: ICLOC fits for the benzene geometry extracted from the crystal structure.

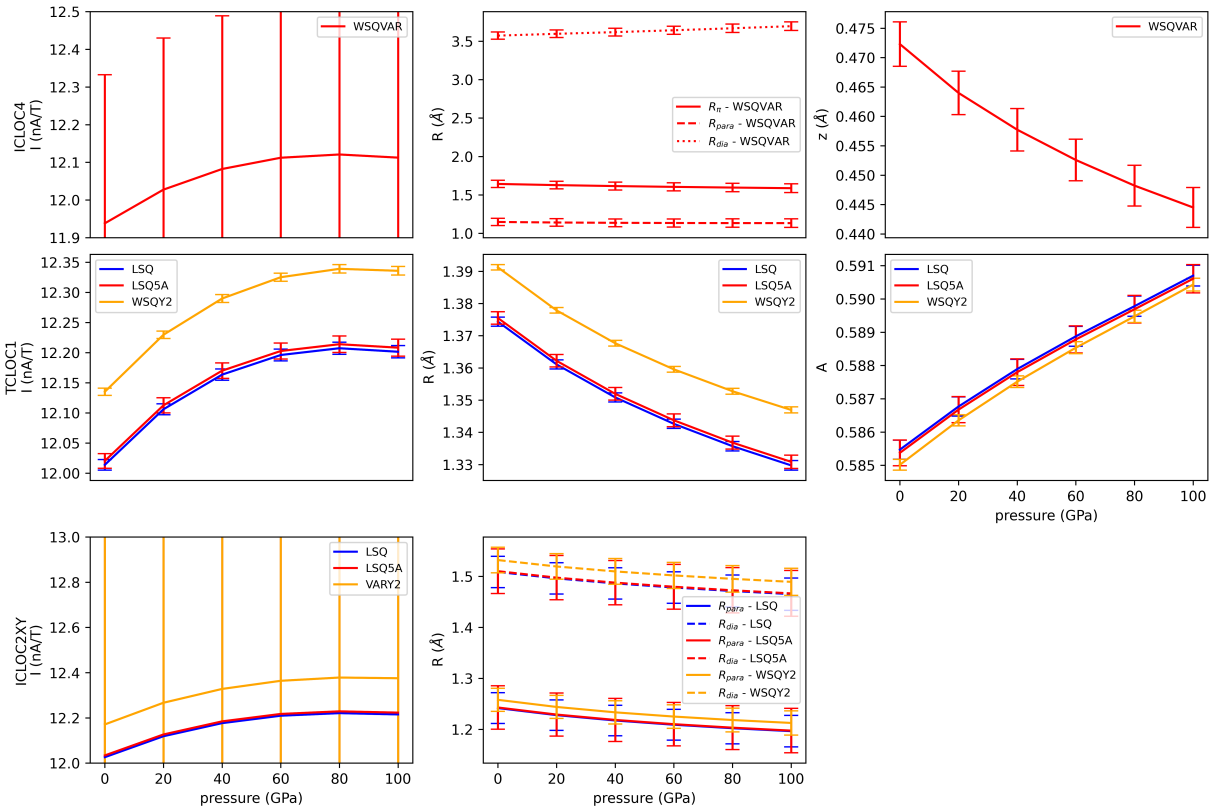

Figure S29: ICLOC parameters for the benzene geometry extracted from the crystal structure.

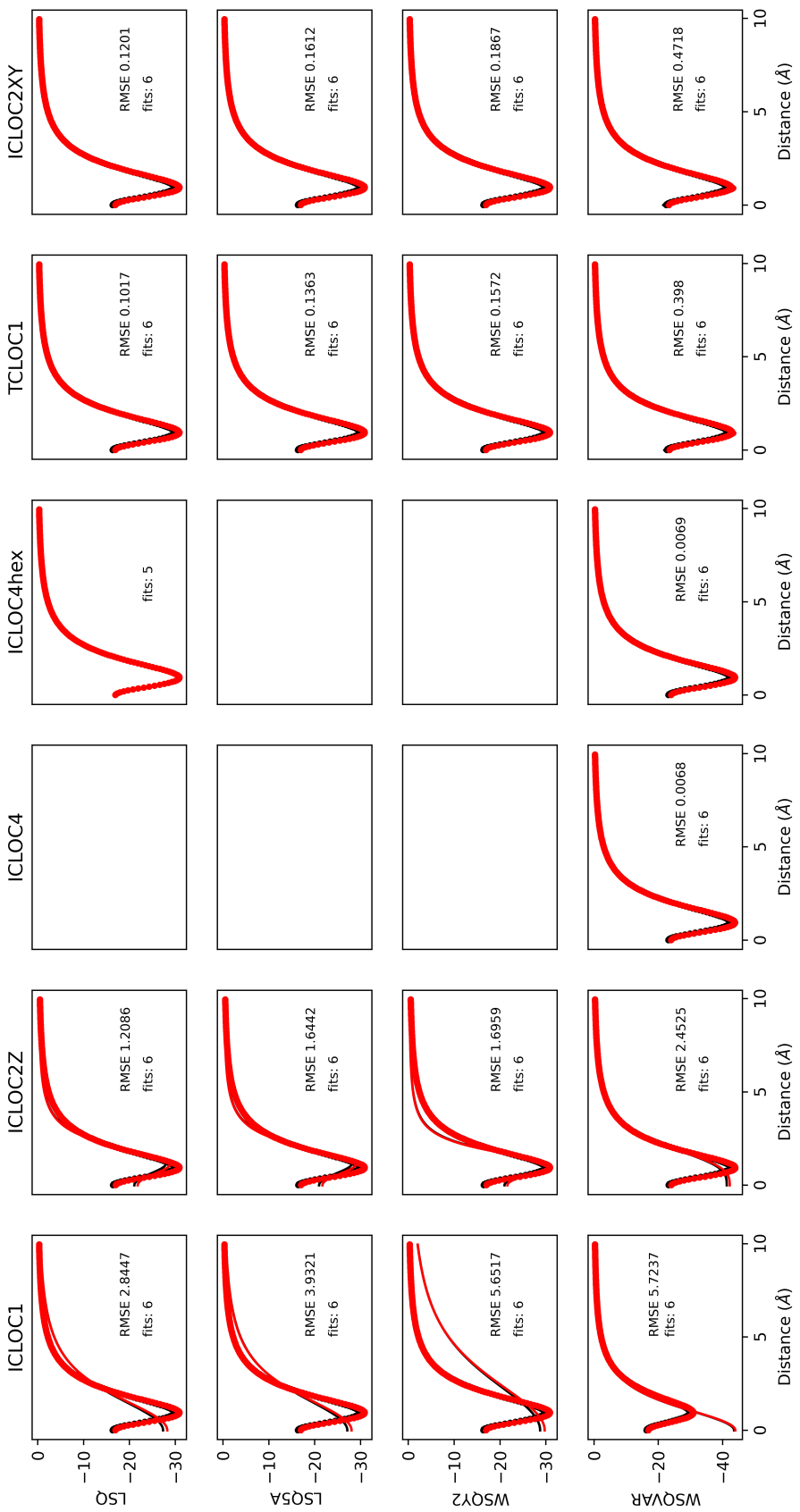

Figure S30: ICLOC fits for the benzene geometry extracted from the crystal structure, followed by a GOSTSHYP electronic structure calculation.

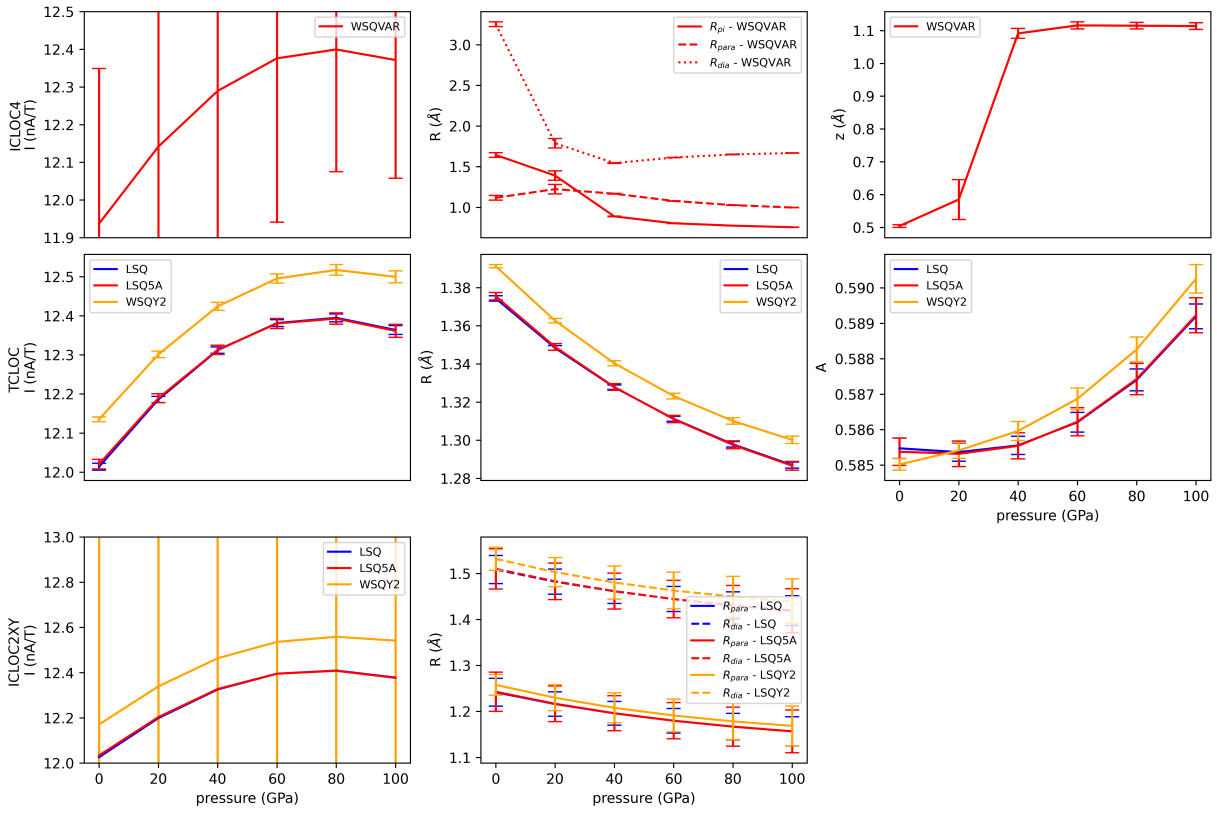

Figure S31: ICLOC parameters for the benzene geometry extracted from the crystal structure, followed by a GOSTSHYP electronic structure calculation.

Finally, the isosurface fitted radii were used with the TCLOC/LSQ model to test the influence of the cavity definition on the results.

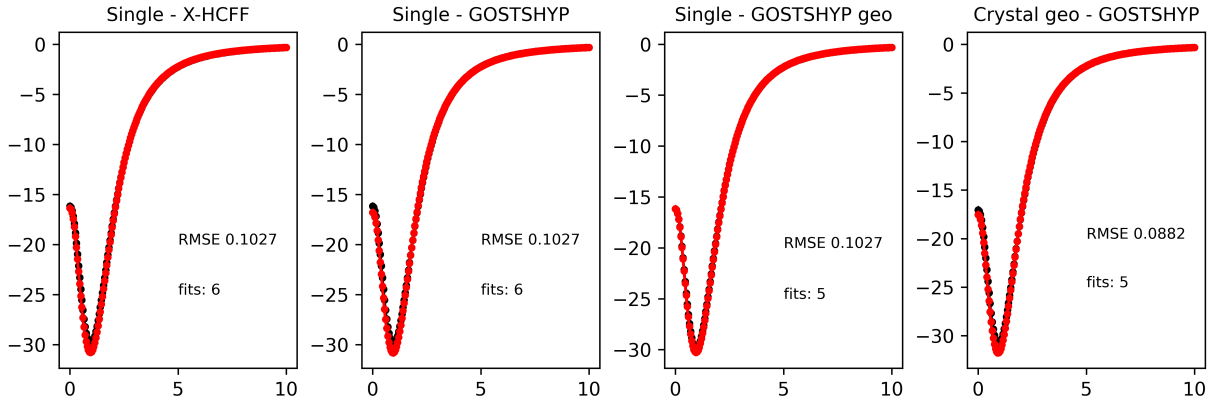

Figure S32: ICLOC fits of the TCLOC/LSQ model with various pressure models using the isosurface fitted radii.

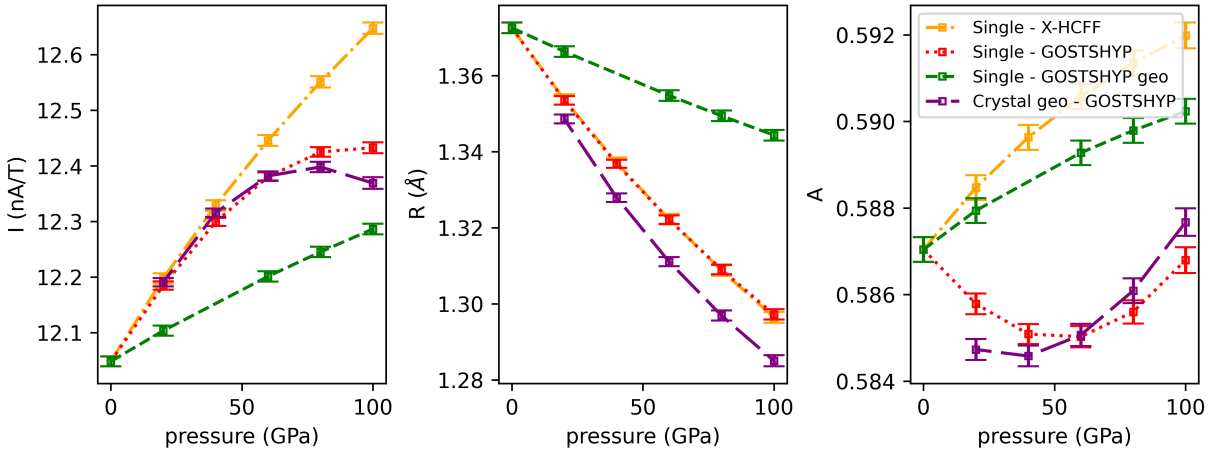

Figure S33: ICLOC parameters of the TCLOC/LSQ model with various pressure models using the isosurface fitted radii.

	X-HCFF		GOSTSHYP		CRYSTAL geo		CRYSTAL GOSTSHYP	
	Dia	Para	Dia	Para	Dia	Para	Dia	Para
0 GPa	11.9 (17.0)	-1.4 (-5.0)	11.9	-1.4	12.1 (16.7)	-1.5 (-4.9)	12.1	-1.5
20 GPa	12.0 (17.2)	-1.5 (-5.0)	12.0	-1.4	11.9 (17.0)	-1.4 (-5.0)	12.0	-1.5
40 GPa	11.9 (17.4)	-1.6 (-5.0)	12.2	-1.5	11.9 (17.1)	-1.5 (-5.0)	11.9	-1.5
60 GPa	11.8 (17.6)	-1.7 (-5.0)	12.6	-1.4	11.8 (17.2)	-1.6 (-5.0)	11.9	-1.5
80 GPa	11.7 (17.7)	-1.7 (-5.0)	13.0	-1.4	11.7 (17.2)	-1.6 (-5.0)	11.8	-1.5
100 GPa	11.6 (17.8)	-1.8 (-5.0)	13.5	-1.4	11.7 (17.2)	-1.6 (-5.1)	11.8	-1.6

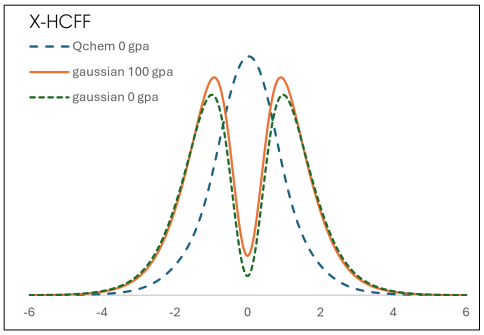

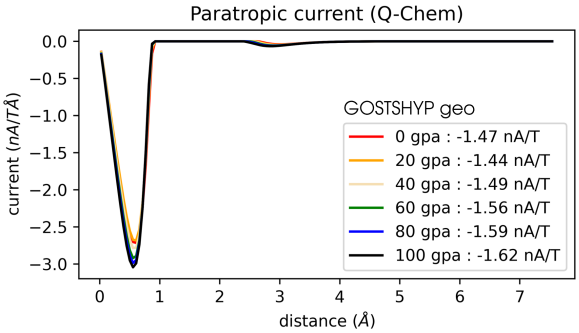

Figure S34: (top) Table containing the results of the GIMIC procedure. (bottom left) Ring current of benzene scanned perpendicular to the molecular plane with Gaussian16 and Q-Chem. (bottom right) Paratropic ring current calculated with Q-Chem.

11 Gauge-Including Magnetically Induced Currents.

GIMIC calculations of the ring current were performed with both Q-Chem and Gaussian. While the Q-Chem calculations reproduced the expected order of magnitude in the shifts in ring current maxima, they were also prone to several problems. These include an underestimation of the magnitude of the diatropic and paratropic ring currents compared to Gaussian16 and the common literature, a nonphysical additional ring current beyond the van der Waals cavity and an erroneous horizontal profile, lacking the characteristic central well due to the paratropic current. For this reason, the Q-Chem results were disregarded in the further analysis in this paper. Below, all numerical results are provided nonetheless and a vertical (left) and horizontal (right) profile of the total (left) and paratropic (right) ring current are provided.

12 Aromaticity Indices - Comparison

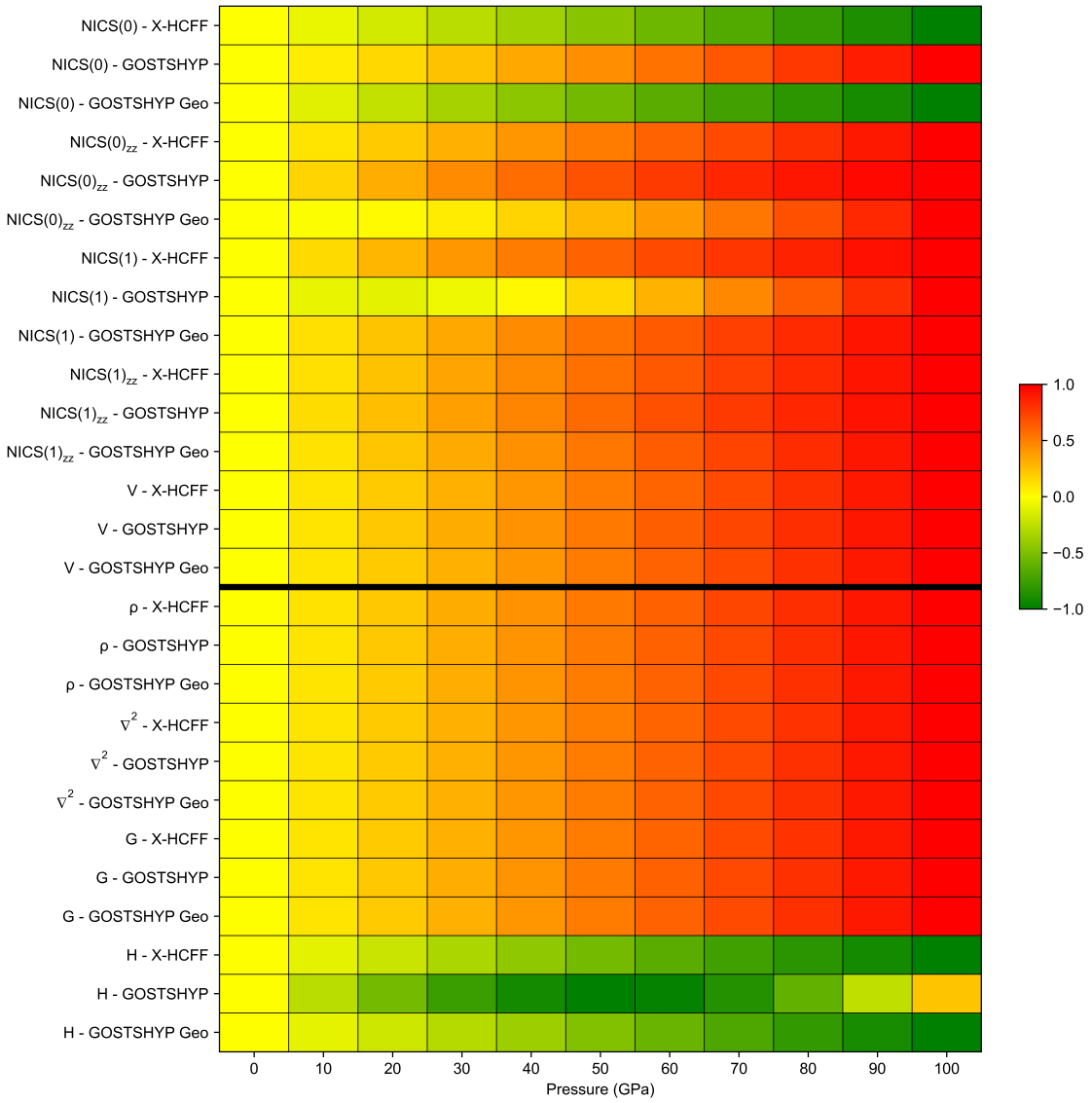

Figure S35: Normalized evolution in aromaticity of the benzene gas phase molecule under pressure at 10 GPa intervals. For each index, normalization is performed with respect to the maximum observed change in aromaticity over the whole pressure range, using the value at 0 GPa as the reference (yellow). An increase in aromaticity is represented by red coloring, whereas a decrease is indicated by green coloring. Descriptors that indicate an increase in aromaticity through a negative gradient are listed above the bold dividing line, while indices that show a positive gradient with increasing aromaticity are listed below.

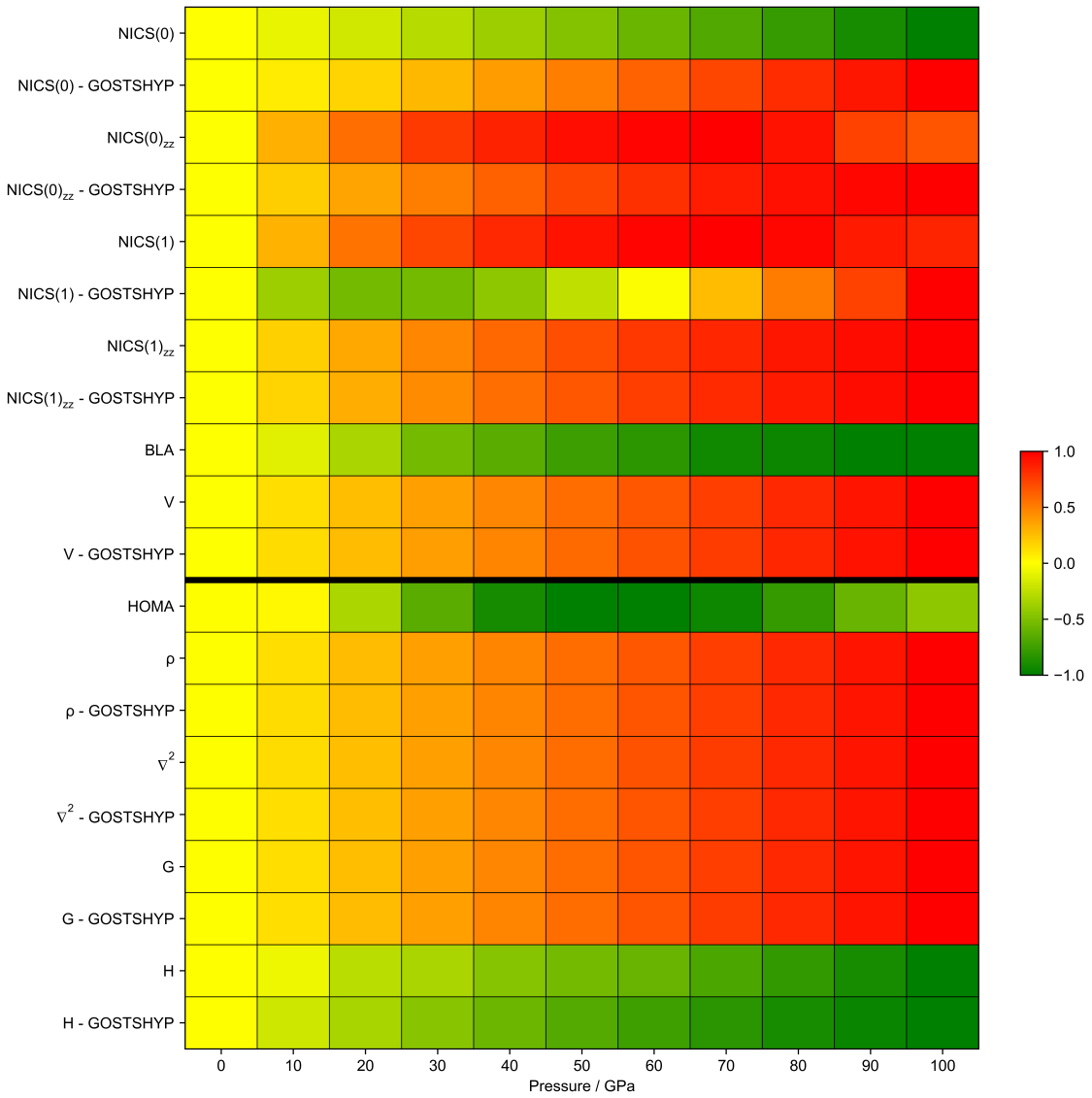

Figure S36: Normalized evolution in aromaticity of the benzene crystal molecule under pressure at 10 GPa intervals. For each index, normalization is performed with respect to the maximum observed change in aromaticity over the whole pressure range, using the value at 0 GPa as the reference (yellow). An increase in aromaticity is represented by red coloring, whereas a decrease is indicated by green coloring. Descriptors that indicate an increase in aromaticity through a negative gradient are listed above the bold dividing line, while indices that show a positive gradient with increasing aromaticity are listed below.

13 Ring Critical Point (RCP) Properties

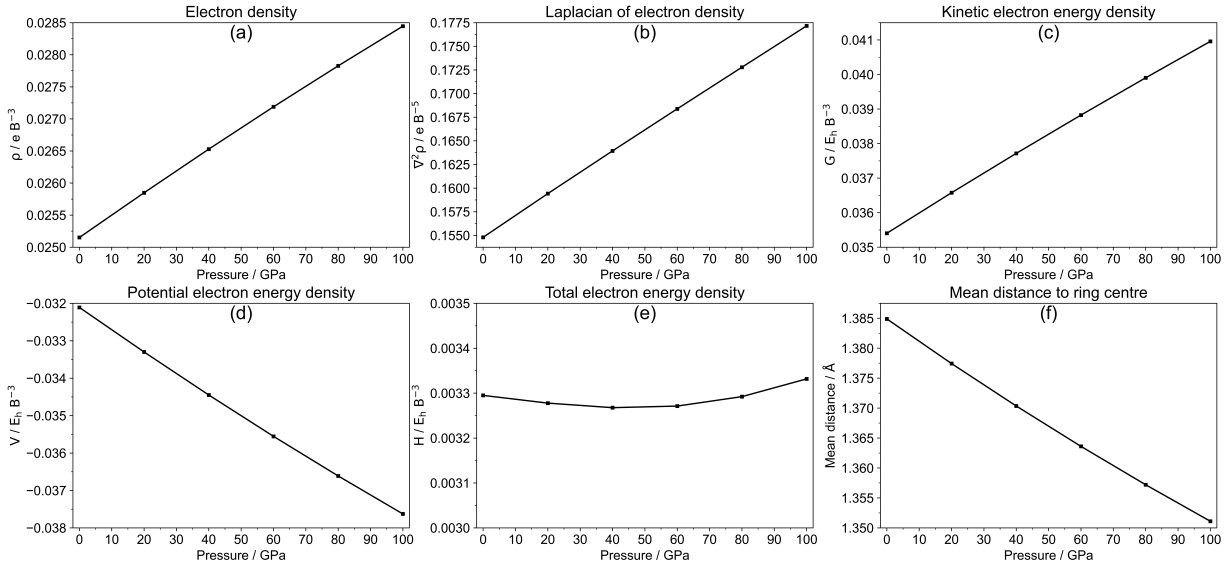

Figure S37: (a) Electron density, (b) Laplacian of electron density, (c) Total electron energy density H, (d) Kinetic electron energy density G and (e) Potential electron energy density V at the RCP of the benzene gas phase molecule with the GOSTSHYP method at the CAM-B3LYP-D3/cc-pVTZ level of theory. (f) Mean distance of each carbon atom to the geometric ring centre of the gas phase molecule.

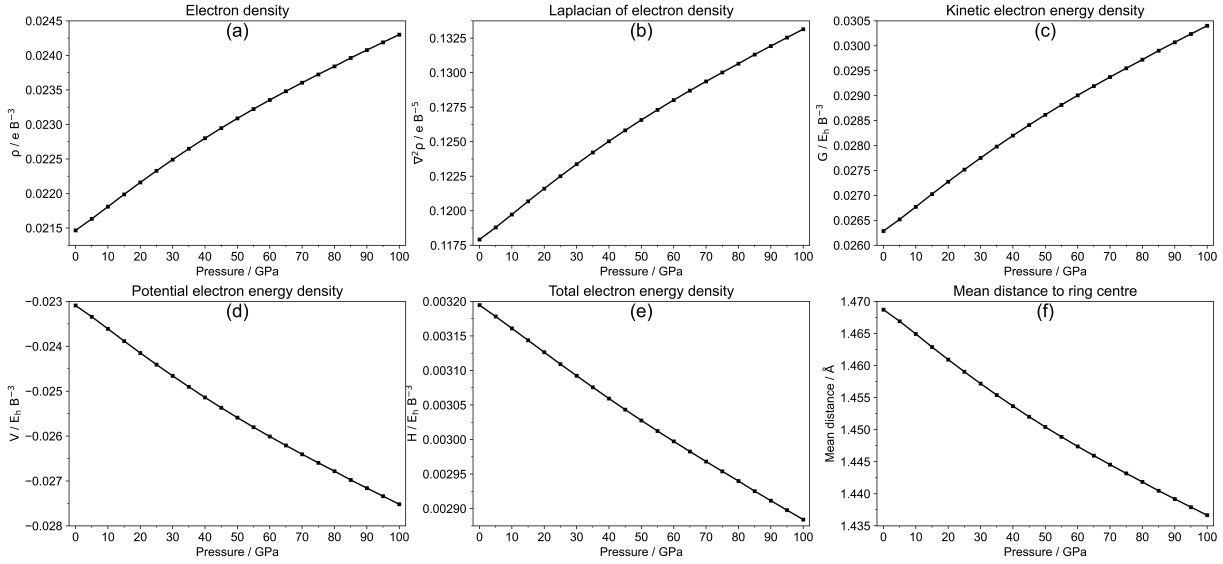

Figure S38: (a) Electron density, (b) Laplacian of electron density, (c) Total electron energy density H, (d) Kinetic electron energy density G and (e) Potential electron energy density V at the RCP of the cyclohexane gas phase molecule with the GOSTSHYP method at the B3LYP-D3/cc-pVTZ level of theory. (f) Mean distance of each carbon atom to the geometric ring centre of the gas phase molecule.

14 Comparison between B3LYP and CAM-B3LYP.

Pressure	B3LYP-D3 - GOSTSHYP				
(GPa)	PDI	I_{ring}	MCI	AV1245	AV_{min}
0	0.103879	0.0474	0.0710	10.48	10.48
20	0.103773	0.0469	0.0703	10.41	10.41
40	0.103721	0.0466	0.0698	10.37	10.36
60	0.103690	0.0464	0.0695	10.33	10.33
80	0.103688	0.0462	0.0693	10.31	10.31
	CAM-B3LYP-D3 - GOSTSHYP				
	PDI	I_{ring}	MCI	AV1245	AV_{min}
0	0.103757	0.0473	0.0709	10.50	10.50
20	0.103605	0.0469	0.0704	10.44	10.42
40	0.103512	0.0466	0.0700	10.40	10.37
60	0.103455	0.0464	0.0697	10.37	10.33
80	0.103422	0.0463	0.0695	10.35	10.30
	B3LYP-D3 - X-HCFF				
	PDI	I_{ring}	MCI	AV1245	AV_{min}
0	0.103878	0.0474	0.0710	10.48	10.48
20	0.104209	0.0466	0.0698	10.34	10.34
40	0.104480	0.0459	0.0686	10.20	10.20
60	0.104701	0.0452	0.0676	10.07	10.07
80	0.104875	0.0447	0.0666	9.94	9.94
	CAM-B3LYP-D3 - X-HCFF				
	PDI	I_{ring}	MCI	AV1245	AV_{min}
0	0.103757	0.0473	0.0709	10.50	10.50
20	0.104094	0.0466	0.0698	10.36	10.36
40	0.104377	0.0459	0.0687	10.23	10.23
60	0.104610	0.0453	0.0677	10.11	10.10
80	0.104799	0.0447	0.0668	9.98	9.98

Table S6: PDI and multicenter aromaticity descriptors of benzene from 0 to 100 GPa with the B3LYP-D3 and CAM-B3LYP-D3 functionals.

15 Comparison of Benzene to Its Antiaromatic Ions Benzene^{2-} and Benzene^{2+}

An example of an antiaromatic molecule can be found in the dication and dianion of benzene, of which the singlet states are known to be antiaromatic. The evolution of the aromaticity indices (RCP, HOMA and multicenter indices) with pressure for these compounds are provided below. Compared to the aromatic triplet state of these systems, the relative change in the various aromaticity indices is comparable in magnitude to slightly higher for the antiaromatic compounds.

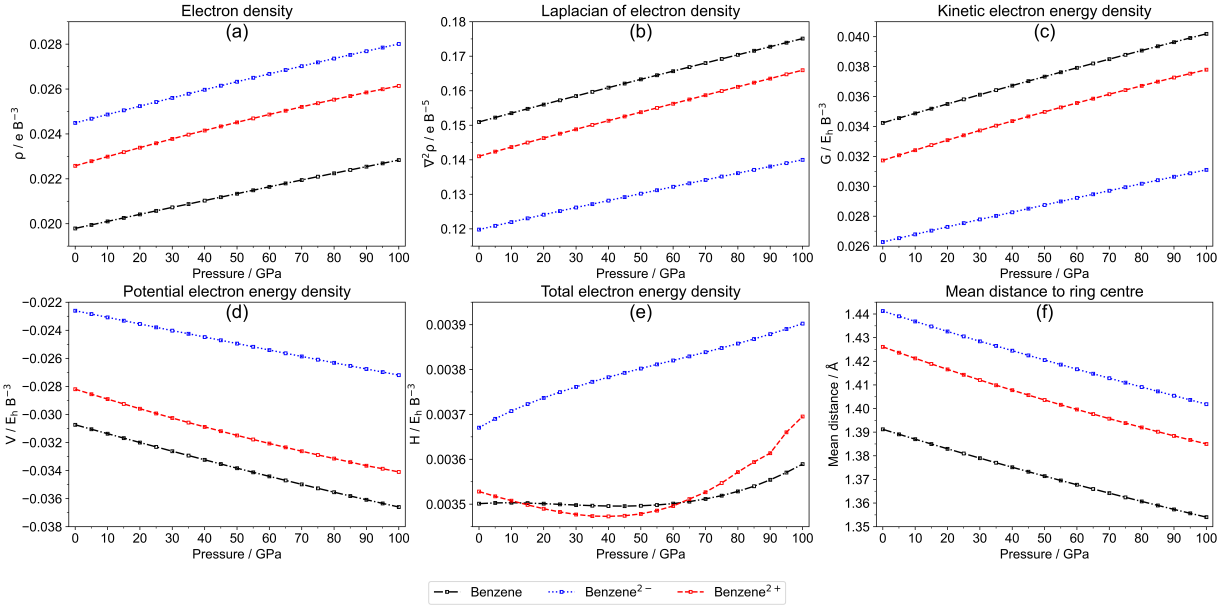

Figure S39: (a) Electron density, (b) Laplacian of electron density, (c) Total electron energy density H, (d) Kinetic electron energy density G and (e) Potential electron energy density V at the RCP of benzene, benzene^{2-} and benzene^{2+} in the triplet state with the GOSTSHYP method at the B3LYP-D3/cc-pVTZ level of theory using a scaling factor of 1.3. (f) Mean distance of each carbon atom to the geometric ring centre.

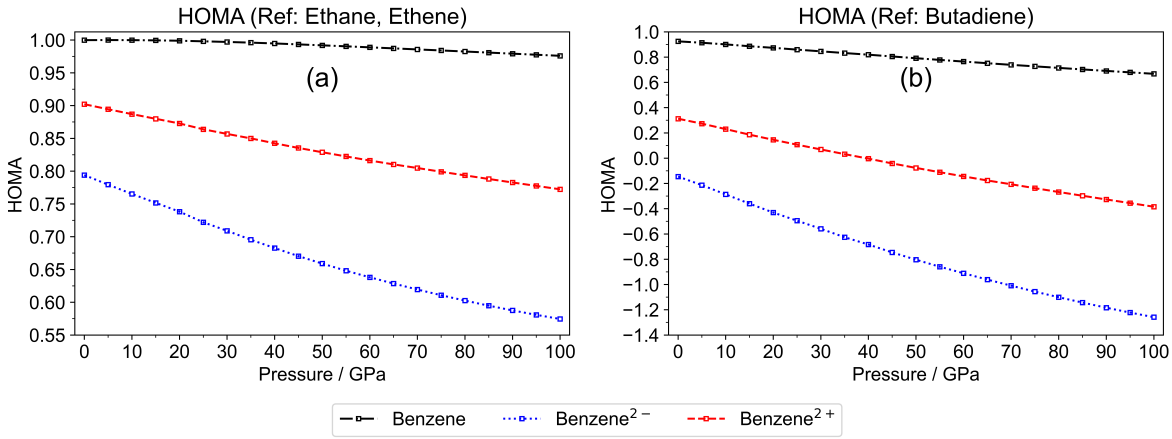

Figure S40: HOMA indices of benzene, benzene^{2-} and benzene^{2+} in the triplet state using ethane and ethene as reference systems. The optimizations were performed with the GOSTSHYP method at the B3LYP-D3/cc-pVTZ level of theory using a scaling factor of 1.3.

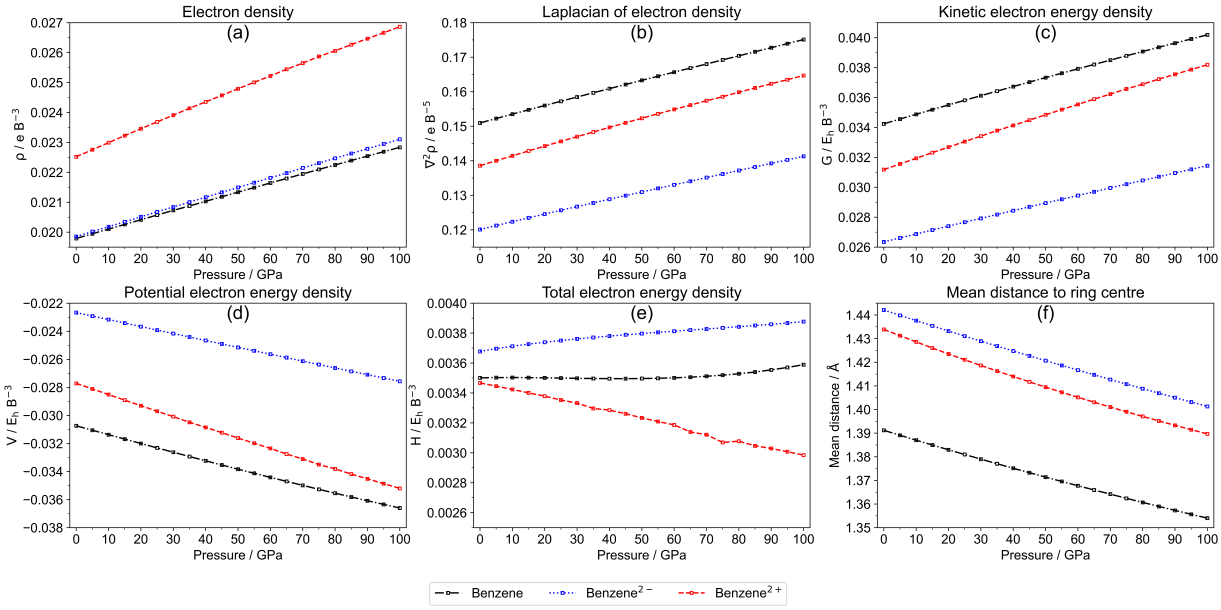

Figure S41: (a) Electron density, (b) Laplacian of electron density, (c) Total electron energy density H, (d) Kinetic electron energy density G and (e) Potential electron energy density V at the RCP of benzene, benzene^{2-} and benzene^{2+} in the singlet state with the GOSTSHYP method at the B3LYP-D3/cc-pVTZ level of theory using a scaling factor of 1.3. (f) Mean distance of each carbon atom to the geometric ring centre.

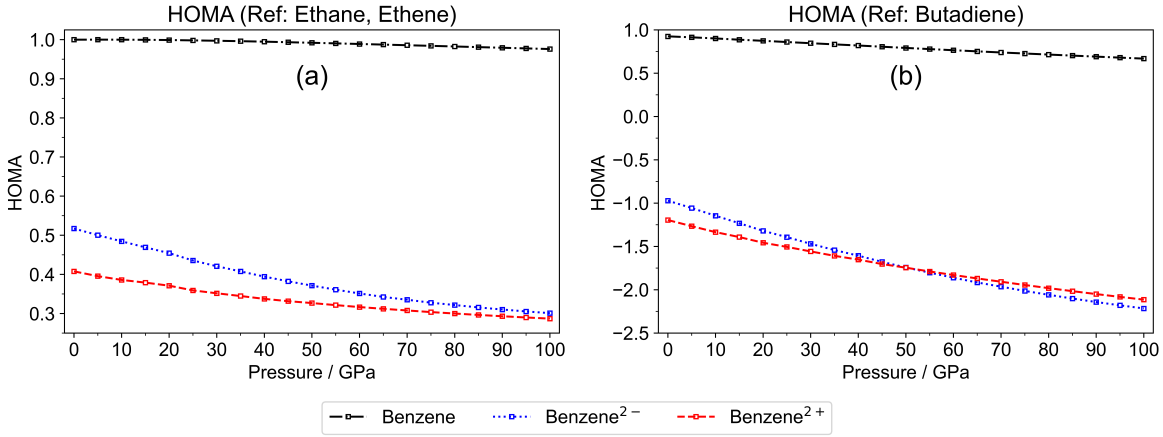

Figure S42: HOMA indices of benzene, benzene^{2-} and benzene^{2+} in the singlet state using ethane and ethene as reference systems. The optimizations were performed with the GOSTSHYP method at the B3LYP-D3/cc-pVTZ level of theory using a scaling factor of 1.3.

		0 GPa	20 GPa	40 GPa	60 GPa	80 GPa	100 GPa
0 Singlet	MCI	0.0709	0.0703	0.0698	0.0695	0.0693	
	I_{ring}	0.0473	0.0469	0.0466	0.0463	0.0462	
	AV1245	10.48	10.41	10.36	10.33	10.31	
	AV_{min}	10.48	10.41	10.36	10.33	10.30	
2+ Singlet	MCI	-0.0128	-0.0131	-0.0134	-0.0137		
	I_{ring}	0.0027	0.0028	0.0028	0.0028		
	AV1245	-1.13	-1.12	-1.10	-1.09		
	AV_{min}	-3.26	-3.26	-3.26	-3.26		
2+ Triplet	MCI	0.0781	0.0780	0.0780	0.0781		
	I_{ring}	0.0275	0.0274	0.0274	0.0274		
	AV1245	11.65	11.64	11.64	11.65		
	AV_{min}	11.65	11.64	11.64	11.65		
2- Singlet	MCI	0.0031	0.0031	0.0031	0.0031	0.0030	0.0030
	I_{ring}	0.0039	0.0038	0.0038	0.0037	0.0037	0.0036
	AV1245	1.05	1.03	1.00	0.98	0.95	0.93
	AV_{min}	-0.78	-0.79	-0.80	-0.82	-0.84	-0.87
2- Triplet	MCI	0.0400	0.0392	0.0386	0.0381	0.0377	0.0374
	I_{ring}	0.0223	0.0219	0.0216	0.0214	0.0212	0.0210
	AV1245	6.55	6.45	6.38	6.32	6.27	6.24
	AV_{min}	6.55	6.45	6.37	6.32	6.27	6.23

Table S7: Multicenter indices of the neutral benzene molecule, the dication (singlet and triplet state) and the dianion (singlet and triplet state)

References

1 A. D. Becke, *J. Chem. Phys.*, 1993, **98**, 5648–5652.

2 P. J. Stephens, F. J. Devlin, C. F. Chabalowski, and M. J. Frisch, *J. Phys. Chem.*, 1994, **98**, 11623–11627.

3 S. Grimme, J. Antony, S. Ehrlich, and H. Krieg, *J. Chem. Phys.*, 2010, **132**, 154104.

4 T. H. Dunning Jr, *J. Chem. Phys.*, 1989, **90**, 1007–1023.

5 T. Stauch, *J. Chem. Phys.*, 2020, **153**, 134503.

6 J. Bentrup, R. Weiß, F. Zeller, and T. Neudecker, *J. Comput. Chem.*, 2025, **46**, e70024.

7 M. Scheurer, A. Dreuw, E. Epifanovsky, M. Head-Gordon, and T. Stauch, *J. Chem. Theory Comput.*, 2020, **17**, 583–597.

8 F. Zeller, E. Berquist, E. Epifanovsky, and T. Neudecker, *J. Chem. Phys.*, 2022, **157**, 184802.

9 E. Epifanovsky, A. T. Gilbert, X. Feng, J. Lee, Y. Mao, N. Mardirossian, P. Pokhilko, A. F. White, M. P. Coons, A. L. Dempwolff et al., *J. Chem. Phys.*, 2021, **155**, 084801.

10 J. Eeckhoudt, M. Alonso, P. Geerlings, and F. De Proft, *J. Chem. Theory Comput.*, 2024, **20**, 7430–7442.

11 G. Van Rossum, *Python 3 Reference Manual*, CreateSpace, 2009.

12 A. v. Bondi, *J. Phys. Chem.*, 1964, **68**, 441–451.

13 G. Kresse and J. Furthmüller, *Phys. Rev. B*, 1996, **54**, 11169.

14 G. Kresse and J. Hafner, *Phys. Rev. B*, 1993, **47**, 558.

15 A. Katrusiak, M. Podsiadło, and A. Budzianowski, *Crystal growth & design*, 2010, **10**, 3461–3465.

16 J. P. Perdew, K. Burke, and M. Ernzerhof, *Phys. Rev. Lett.*, 1996, **77**, 3865.

17 P. E. Blöchl, *Phys. Rev. B*, 1994, **50**, 17953.

18 G. Kresse and D. Joubert, *Phys. Rev. B*, 1999, **59**, 1758.

19 M. K. Cyrański and T. M. Krygowski, *Tetrahedron*, 1999, **55**, 6205–6210.

20 C. H. Choi and M. Kertesz, *J. Chem. Phys.*, 1998, **108**, 6681–6688.

21 T. Lu and F. Chen, *J. Comput. Chem.*, 2012, **33**, 580–592.

22 I. F. Perepichka and D. F. Perepichka, *Handbook of Thiophene-Based Materials: Applications in Organic Electronics and Photonics, 2 Volume Set*, John Wiley & Sons, 2009.

23 J. Kruszewski and T. Krygowski, *Tetrahedron Lett.*, 1972, **13**, 3839–3842.

24 T. M. Krygowski, *J. Chem. Inf. Comput. Sci.*, 1993, **33**, 70–78.

25 R. F. Bader, *Chem. Rev.*, 1991, **91**, 893–928.

26 R. F. Bader, *Atoms in Molecules: A Quantum Theory*, Clarendon Press, 1994.

27 S. Howard and T. Krygowski, *Can. J. Chem.*, 1997, **75**, 1174–1181.

28 M. Palusiak and T. M. Krygowski, *Chem. Eur. J.*, 2007, **13**, 7996–8006.

29 T. A. Keith, *TK Gristmill Software: Overland Park, KS, USA*, 2019, **23**.

30 E. Matito, *ESI-3D: Electron Sharing Indices Program for 3D Molecular Space Partitioning*, 2006, Institute for Computational Chemistry and Catalysis, University of Girona.

31 F. L. Hirshfeld, *Theor. Chim. Acta*, 1977, **44**, 129.

32 P. Salvador and E. Ramos-Cordoba, *J. Chem. Phys.*, 2013, **139**.

33 P. Salvador, E. Ramos-Cordoba, M. Montilla, L. Pujal, and M. Gimferrer, *J. Chem. Phys.*, 2024, **160**, 172502.

34 B. Wang, P. Geerlings, C. Van Alsenoy, F. Heider-Zadeh, P. W. Ayers, and F. De Proft, *J. Chem. Theory Comput.*, 2023, **19**, 3223–3236.

35 P. v. R. Schleyer, C. Maerker, A. Dransfeld, H. Jiao, and N. J. van Eikema Hommes, *J. Am. Chem. Soc.*, 1996, **118**, 6317–6318.

36 Z. Chen, C. S. Wannere, C. Corminboeuf, R. Puchta, and P. v. R. Schleyer, *Chem. Rev.*, 2005, **105**, 3842–3888.

37 H. Fallah-Bagher-Shaidaei, C. S. Wannere, C. Corminboeuf, R. Puchta, and P. v. R. Schleyer, *Org. Lett.*, 2006, **8**, 863–866.

38 C. Johnson and F. Bovey, *J. Chem. Phys.*, 1958, **29**, 1012–1014.

39 J. A. Pople, *J. Chem. Phys.*, 1956, **24**, 1111–1112.

40 J. Waugh and R. Fessenden, *J. Am. Chem. Soc.*, 1957, **79**, 846–849.

41 J. Kussmann, *Convert Output of Q-Chem or FermiONs++ for GIMIC (TURBOMOLE format)*, 2016, Faculty for Chemistry and Pharmacy, Ludwig Maximilian University of Munich.

42 T. Yanai, D. P. Tew, and N. C. Handy, *Chem. Phys. Lett.*, 2004, **393**, 51–57.

43 T. M. Krygowski, H. Szatylowicz, O. A. Stasyuk, J. Dominikowska, and M. Palusiak, *Chem. Rev.*, 2014, **114**, 6383–6422.